Triggering of the 2012 Ahar-Varzaghan earthquake doublet (Mw6.5&6.3) by the Sahand Volcano and North Tabriz fault (NW-Iran); Implications on the seismic hazard of Tabriz city

Seyyedmaalek Momeni[1]

[1]EPFL, Geo-Energy Lab – Gaznat Chair on Geo-Energy

November 22, 2022

Abstract

Seismic history of the North Tabriz fault (NTF), the main active fault of Northwestern Iran near Tabriz city, and its relation to the Sahand active Volcano (SND), the second high mountain of the NW Iran, and to the 11 August 2012 Ahar-Varzaghan earthquake doublet (Mw6.5&6.3) (AVD), is investigated. I infer that before AVD seismicity of the central segment of NTF close to SND was very low compared to its neighbor segments. Magmatic activities and thermal springs near central NTF close to Bostan-Abad city and low-velocity anomalies reported beneath SND toward NTF in tomography studies suggest that the existing heat due to SND magma chamber has increased the pore-fluid pressure that overcomes the effective normal stress on the central NTF, resulting in its creep behaviour. Two peaks of cumulative scalar seismic moments of earthquakes observed on both lobes of the creeping segment, confirming the strong difference in the deformation rate between these segments. On 2012, AVD struck in the 50 km North of NTF, in the same longitude range to SND and with the same right-lateral strike-slip mechanism to 1 1 2 3 4 5 6 7 8 9 10 11 12 13 14 15 16 17 18 19 20 21 22 23 NTF, as a result of partial transfer of the right-lateral deformation of NW Iran toward the North of NTF on the Ahar-Varzaghan fault system. A cumulative aseismic slip equal to an Mw6.8 event is estimated for the creeping segment of NTF, posing half of the 7mmy-1 geodetic deformation has happened in the creep mode. This event has transferred a positive Coulomb stress field of >1 bar on the AVD and triggered them. Also, the western and eastern NTF segments received >4 bar of positive Coulomb stresses from the creeping segment and are probable nucleation locations for future earthquakes on NTF. The observed creep may be the reason for the NTF segmentation during the 1721AD M7.6 and 1780 AD M7.4 historical earthquakes.

Triggering of the 2012 Ahar-Varzaghan earthquake doublet (Mw6.5&6.3) by the Sahand Volcano and North Tabriz fault (NW-Iran); Implications on the seismic hazard of Tabriz city

Seyyedmaalek Momeni[1,2*]

1. EPFL Geo-Energy Lab – Gaznat Chair on Geo-Energy, EPFL-ENAC-IIC-GEL, Station 18, CH-1015, Lausanne, Switzerland.

2. International Centre for Theoretical Physics (ICTP), Trieste, Italy.

* Corresponding author, E-mail: maalek.momeni@gmail.com

Abstract

Seismic history of the North Tabriz fault (NTF), the main active fault of Northwestern Iran near Tabriz city, and its relation to the Sahand active Volcano (SND), the second high mountain of the NW Iran, and to the 11 August 2012 Ahar-Varzaghan earthquake doublet (Mw6.5&6.3) (AVD), is investigated. I infer that before AVD seismicity of the central segment of NTF close to SND was very low compared to its neighbor segments. Magmatic activities and thermal springs near central NTF close to Bostan-Abad city

and low-velocity anomalies reported beneath SND toward NTF in tomography studies suggest that the existing heat due to SND magma chamber has increased the pore-fluid pressure that overcomes the effective normal stress on the central NTF, resulting in its creep behaviour. Two peaks of cumulative scalar seismic moments of earthquakes observed on both lobes of the creeping segment, confirming the strong difference in the deformation rate between these segments. On 2012, AVD struck in the 50 km North of NTF, in the same longitude range to SND and with the same right-lateral strike-slip mechanism to NTF, as a result of partial transfer of the right-lateral deformation of NW Iran toward the North of NTF on the Ahar-Varzaghan fault system. A cumulative aseismic slip equal to an Mw6.8 event is estimated for the creeping segment of NTF, posing half of the 7mmy-1 geodetic deformation has happened in the creep mode. This event has transferred a positive Coulomb stress field of >1 bar on the AVD and triggered them. Also, the western and eastern NTF segments received >4 bar of positive Coulomb stresses from the creeping segment and are probable nucleation locations for future earthquakes on NTF. The observed creep may be the reason for the NTF segmentation during the 1721AD M7.6 and 1780 AD M7.4 historical earthquakes.

Keywords: Induced seismicity; aseismic deformation; pore-fluid pressure; effective stress; volcano; triggering

1. Introduction

On 11 August 2012, an earthquake doublet with Mw6.5 and Mw6.3 occurred in NW Iran near the Ahar and Varzaghan cities (AVD), 40 km Northeast of Tabriz city (TBZ), the fourth megacity of Iran with >2 million population. They located in 50 km North of Sahand Volcano (SND), which situated 40 km Southeast of TBZ. AVD caused >300 fatalities. In terms of mechanism, the first mainshock exhibits an almost pure right-lateral strike-slip faulting, and the second one had two slip patches with right-lateral strike-slip and reverse mechanisms (Fig. 1a, Momeni & Tatar, 2018; Momeni et al, 2019). The first mainshock produces almost 12 km of surface rupture. The mainshocks mechanisms and their rupture geometries were almost the same to the North Tabriz Fault (NTF), the main active fault of northwestern Iran, that crosses just North of TBZ. Before AVD, the seismicity on the Ahar-Varzaghan fault system was negligible, so that these events were a surprise in that region.

Tectonic Settings

NW of Iran is a part of Turkish-Iranian plateau, bounded by the Caucasus Mountains to the North, Zagros Fold and thrust belt to the South, and Talesh Mountains to the East. This region is under complex tectonics which resulted in high deformation and seismic activity (Berberian and Arshadi, 1976; Jackson, 1992; Ghods et al., 2015; Momeni & Tatar, 2018) (Fig. 1). The main tectonic regime is the oblique convergence of Arabia-Eurasia with the current deformation rate of about 13–15 mmy-1, at the longitude of 46.1 °E (Vernant et al., 2004; Reilinger et al., 2006). The Talesh Mountains on the eastern termination of the region is either colliding to the relatively thick South Caspian sedimentary cover (20 km) (Zamani and Masson, 2014) or, the South Caspian crust is under-thrusting westward beneath it (Jackson et al., 2002). Two different northeastward and northwestward deformation directions are observable in the GPS velocity vectors at the longitude of 44degE, which suggest it as the western margin of the region (Momeni & Tatar, 2018).

Earthquakes mechanisms (GCMT) and surface deformation studies (Reilinger et al., 2006; Djamour et al., 2011) suggest the resulting deformation in NW Iran is mainly the right-lateral strike-slip faulting on the W-NW striking faults within the region. While thrust faulting is partitioned to the North on the Great Caucasus (Jackson, 1992; McClusky et al., 2000; Momeni & Tatar, 2018). The two N-S to NE-SW (N018deg) shortening and NW-SE (N287deg and N155deg) strike-slip deformation stress regimes were obtained by Zamani and Masson, (2014). The first stress system developed the three E-W striking fold and thrust belts, Arasbaran, Ghoshe-dagh and Bozkosh mountain ranges. While the N-S striking structures like Talesh mountains corresponds to the second stress system (Fig. 1a).

NTF with the main right-lateral strike-slip mechanism and deformation rate of 7 +- 1 mmy-1 accommodates most of the deformation of the region (Djamour et al., 2011). Rizza et al., (2013) estimated that the current deformation rate has been mostly constant since late quaternary until now (during the past 45 ka). However, they remarked a decrease in the strike-slip deformation rates along the NTF from about 7 mmy-1 to 5 mmy-1 from the West to the East of 47deg longitude, and they relate it to the fault orientation changes from about NW-SE to W-E (Djamour et al., 2011; Rizza et al., 2013) (Fig. 2a). Later, Su et al., (2017) reported subsidence in the closest GPS station to the Northeast SND near BA and interpreted it as magmatic activities of Sahand.

A microseismicity study along the NTF using a local seismic network confirmed the main shear deformation mechanism of NTF in the upper crust (Moradi et al. 2011). On the western and eastern terminations of NTF, the North Mishu Fault (NMF) and the South Bozkosh Fault (SBF) are the two oblique reverse faults with right-lateral strike-slip components that strike ˜E-W and dip to the South and North, respectively. Solaymani Azad et al., (2015) called the NTF, NMF, and SBF as Tabriz Fault System (TFS).

Before the occurrence of the 2012 earthquake doublet, the Ahar-Varzaghan fault system has been in a long seismic quiescence (Momeni & Tatar, 2018; Fig. 1a). However, field observations revealed the continuation of fault to the both East and West of the ruptured segment during the 2012 AVD (e.g. Copley et al. 2013, Donner et al. 2015, Ghods et al. 2015). The clear segmentation has been observed along this fault system with different kinematics and without clear connections that suggest it as a young fault system (Donner et al., 2015). The occurrence of the AVD suggested that some of the shear strain of the region is not compensating by the NTF, specifically at the longitudes east of 46degE (Donner et al. 2015; Ghods et al. 2015).

Sahand volcano with 3707 m elevation is an isolated, extensively distributed (˜3000 km2 area) stratovolcanic complex (Ghalamghash et al., 2019). Together with Sabalan and Saray, they are three Late Miocene-Quaternary volcanoes that formed as results of the collision between the Arabian and Eurasian plates along the Neo-Tethyan suture zone in NW Iran. The formation of Neo-Sahand is estimated to ca. 600 to b173 ka (Ghalamghash et al., 2019). They mostly observed within and outside of the widely eroded caldera margin. Neo-Sahand units include basaltic andesitic to rhyolitic domes in the center of the complex as well as small parasitic cones along with subvolcanic dikes toward the northeast.

Historical earthquakes of NW Iran

Historical seismicity is widely distributed in the region, and mostly on the NTF and NMF. Tabriz city has been the capital of Iran and Azerbaijan in the past. Several large destructive historical earthquakes (magnitudes up to Ms=7.6) have reported for Tabriz (Ambraseys and Melville, 1982; Berberian and Yeats, 1999). Most of them are related to the activity of NTF (Fig. 1a). The last two M>7 destructive historical earthquakes have occurred on 1721 AD and 1780 AD, that ruptured more than 50 km of the southeastern and northwestern segments of the NTF and caused over 40,000 and 200,000 fatalities, respectively (Ambraseys and Melville, 1982; Berberian and Yeats, 1999; Momeni & Tatar, 2018).

Paleoseismological studies revealed at least three major (M 7.5) historical earthquakes for the southeastern segment over the past 33.5 ka, including the 1721 AD M7.6–7.7 earthquake (Solaymani Azad et al., 2015). On the other side, four historical earthquakes are reported for the northwestern segment of the NTF during the past 3.6 ka, the most recent being the Ms 7.4 1780 AD earthquake (Hessami Azar et al., 2003). The estimated slip per event and slip rate on this segment are 4 +- 0.5 m and 3.1–6.4 mmy-1, respectively, and the average recurrence interval of large earthquakes on it is estimated in the range of 350 to 1430 years.

NMF and SBF also ruptured during historical earthquakes, the last two being the 1786 AD Marand and 1593 AD Sarab earthquakes that suggest a seismic migration from the southeast toward the northwest of TFS. They also reveal earthquake clustering (e.g. Kagan and Jackson, 1991; Berberian, 1997; Karakhanian et al., 2004) and interaction between fault segments of the TFS (Solaymani Azad et al., 2015).

Instrumental earthquakes of NW Iran

Mechanism of deformation strongly changes from the western Alborz to the Iran-Turkey borders. The 1976 Mw7.0 Chalderan earthquake has occurred near the borders of Iran with Turkey on the right-lateral strike-slip Chalderan-Khoy fault that strikes E-W. While, the 1990 Mw7.4 Rudbar-Tarom earthquake on the western

Alborz mountains has occurred on a left-lateral strike-slip fault trending WNW- ESE (Momeni & Tatar, 2018).

Within the NW Iran before the AVD, the 1997 Mw = 6.1 Ardebil earthquake occurred on an N-S striking fault situated ~150 km East of the AVD, showing a pure left-lateral strike-slip faulting (Aziz Zanjani et al., 2013). On 11 August 2012, the AVD occurred that were very well recorded by different instruments. The first mainshock with Mw6.5 had a right-lateral strike-slip mechanism. While the second one with Mw6.3 was more complex and contained two slip patches: the first patch had a right-lateral strike-slip mechanism, and the second one had a reverse mechanism (Momeni et al., 2019). The last large earthquake in the region is the 7 November 2019 Mw5.9 Torkamanchay earthquake (TKC) that occurred on an NE striking left-lateral strike-slip fault between North and South Bozkosh Faults (Valerio et al., 2020).

The EHB catalog (Engdahl et al., 2006) shows most of the seismicity on the Talesh mountains and also on the NMF (Fig. 1a). However, no large earthquake (M>5) reported on the segments of NTF in the GCMT catalog (Fig. 1b).

In 1995 a local permanent seismic network consisting of eight stations, known as Tabriz sub-network of the Iranian Seismological Center (IRSC), was installed in the region (Fig. 1b). However, this sparse network (station spacing ~50 km) limited the number of precisely located earthquakes. There are only 70 earthquakes in IRSC catalog from 1995 until the end of 2005, and none of them has located close (distance <5km) to NTF. From 2006, after the installation of the Broadband Iranian Network (BIN) maintained by the International Institute of Earthquake Engineering and Seismology (IIEES) in Tehran, Iran, and improvement of IRSC network data, the IRSC locations improved in terms of accuracy and magnitude completeness.

Figure 1b shows the precisely located seismicity of the region recorded in the IRSC network from 1995 until the occurrence of AVD in August 2012. They have located by at least five stations, have a location error of <5 km, RMS of <0.5 s, and azimuthal gap of <270deg. They are all smaller than Mw5.0 unless the 1997 Ardabil earthquake. They mostly have shallow focal depths (< 20 km) and are distributed mainly along the NTF and NMF. However, the central segment of NTF near SND shows much lower seismic activity compared to the western and eastern segments (Fig. 1b). A seismic cluster on the North of AVD is mainly related to mining activities in that area. The rest of the seismicity is related to the Astaneh (ASF), West Alborz (WAF), South Qoshadagh (SQF), Goshachay (GCF), South Bozkosh (SBF), North Mishu (NMF), Maragheh (MGF), Khajeh (KHF), and Nehram (NHF) faults. After AVD, the only large event of the region is the 7 November 2019 Mw5.9 Torkamanchay earthquake that occurred on an NE striking vertical dip fault between NBF and SBF near the eastern termination of NTF.

Detailed microseismic monitoring on the NTF by a local dense seismic network data confirmed its right-lateral strike-slip mechanism with an East-Southeastward oriented fault plane (Moradi et al., 2011; Fig. 4). Microearthquakes located by Moradi et al., (2011) on NTF situated in the upper crystalline crust at depths shallower than 20 km. Moradi et al. proposed a vertical dip fault plane for the NTF.

The goal

In this study, the seismic activity of the NTF from historical earthquakes until 2020 is investigated. A cumulative slip model has proposed for the creeping segment of NTF near SND, and, the transferred Coulomb stress by this aseismic deformation on the AVD ruptures has computed. Ultimately, the relation between NTF seismic-aseismic deformation activity to SND and AVD, and changes in the rheology of the central segment of NTF near SND after AVD investigated.

Seismicity along NTF and NMF

As mentioned before, earthquake locations by IRSC seismic network in NW Iran started in 1995. However, the IRSC catalog is poor until the end of 2005 due to data quality and sparsely distanced stations (>50 km). There are no earthquakes in the distance of 5 km to the NTF from 1995 to the end of 2005. From 2006, earthquake monitoring has improved in this region in terms of location accuracy and magnitude completeness.

The well-located earthquakes in the distance of 5 km to NTF and NMF are selected from 2006 until before the AVD and from AVD until November 2019 TKC in the IRSC network. These sets are recorded in >=5 stations, with location errors of <5 km, RMS of <0.5 s, and azimuthal gap of < 270deg. The first set contains 512 earthquakes in which 45 of them have magnitudes 2.5 and higher. I infer that the central segment of NTF near SND has a long quiescence from 2006 until the occurrence of AVD. However, the two nearby segments show high seismicity (Fig. 2a).

After AVD, 69 M>=2.5 earthquakes are in 5 km distance to NTF and NMF (IRSC catalog) with a distributed seismicity and their most concentration on the NMF (Fig. 2b; Table S3). However, the two relatively large events (3.7<M<4.0) are located in the central NTF near SND (Fig. 2b).

The cumulative scalar seismic moments of the earthquakes that occurred after 2006 until the 2012 AVD, and after that until TKC, is computed to investigate the seismic energy release behaviour along the NTF and NMF. The cumulative scalar seismic moment plot of the first set shows two peaks in the Eastern and Western lobes of central NTF that matches to SND, and one on the NMF (Fig. 2b). However, the central NTF itself was almost silent.

For earthquakes that occurred on NTF After AVD, the cumulative scalar seismic moment plot shows a peak in the middle of the central NTF. However, the previously observed peaks of the scalar seismic moment on its lobes are disappeared (Fig. 2b). There is also a relatively wide peak on the NMF, North of Urmieh Lake, where the high seismicity was also observed before AVD.

Creeping segment of NTF near SND

Creeping behaviour is mainly related to frictional strength of the fault zone material, depending on lithology, temperature, and pore-fluid pressure (i.e. Avouac, 2015, Khoshmanesh & Shirzaei, 2018). The magmatic activities reported in a GPS study by Su et al., (2017) near BA, known thermal springs there, and absence of seismic activity from 2006 until 2012 AVD on the central NTF near BA, propose that the existing heat due to the SND magma chamber decrease the effective normal stress on this segment of the fault by increasing the pore-fluid pressure on the fractured fault area and consequently cause it to creep. The resulting different deformation rates along NTF segments is probably the reason for the observed two peaks of high cumulative scalar seismic moments on both lobes of central segment of NTF near SND.

To prove this idea, a cumulative aseismic deformation on the central segment of NTF is estimated. This segment didn't rupture since the 1721 M7.6 historical earthquake and the GPS study by Djamour et al., (2011) and Rizza et al., (2013) suggest right-lateral deformation of 7mmy-1 for this segment. A maximum slip of 0.007*(2012-1721) =2.04 meters is expected for this segment until the AVD. This segment has a strike/dip of 300deg/90deg and covers the silent central segment of NTF with a length of ~30 km and locking depth of ~20 km that is suggested by Djamour et al., (2011). I stress that Rizza et al., (2013) suggested a relatively unchanged deformation rate on NTF since 65 ka. If I fairly pose that only half of this deformation has happened in creep mode and the other half is locked (and may rupture in a future earthquake), the slip model will have a maximum value equal to 1.02 m. Later in section 4, I will explain that even considering the smaller contribution of creep in the whole deformation (i.e. 25%), the transferred stress field by the creeping segment will be high enough to trigger the AVD. An elliptical slip patch (i.e. Ruiz & Madariaga, 2013; Momeni et al., 2019) is proposed with a max slip of 1.02 m at the center and with a Gaussian distribution of slip and half of the max slip equal to ~51 cm on the borders, where high seismic activity is observed (Fig. 2a). The resulting source has a scalar seismic moment of ~2.0*e+19 Nm equal to an Mw6.8 earthquake. For a fully creeping slip model, the source will have a scalar seismic moment of ~4.0*e+19 Nm equal to an Mw7.0 earthquake.

The resulting deformation may transfer positive Coulomb failure stresses on the nearby faults. I note that AVD has occurred in the same longitude to this creeping segment, suggesting that the right-lateral deformation does not fully release on NTF and probably some of it transfer toward North, as also suggested by Donner et al., (2015) by geological investigations.

4. Stress transfer

4.1. Stress transfer from the creeping segment of NTF to AVD

The stress tensor produced by the defined slip model for the creeping segment of NTF is calculated on a 3-D grid in the region using a method by Wang et al. (2003) (Fig. 3). The method is based on the dislocation theory that is implemented in a multilayered media. A 1-D crustal velocity model of the area retrieved from precisely located aftershocks of AVD is used, and a Poisson ratio of 0.25 obtained from a Vp/Vs ratio of 1.74 (Momeni & Tatar 2018, Table S1). The Coulomb stress field is calculated on optimally oriented ruptures of both Ahar-Varzaghan earthquakes, and by considering strike-slip mechanisms of their slip patches obtained by Momeni et al., (2019).

A positive Coulomb stress of >1 bar is transferred from the creeping segment on the ruptured areas during the doublet (Fig. 3a). Also, the creeping segment had positive coulomb stress transfer of >4 bar on the nearby segments and excited them to slip (Fig. 3b), especially on the western segment of NTF (e.g., Vadacca, 2020).

4.2. Stress transfer from AVD to NTF

The stress tensor produced by the AVD ruptures that were obtained in a study by Momeni et al., (2019) is computed on the region using the same method mentioned in section 4.1. As was also reported by Momeni et al., (2019), the stress field shows a positive Coulomb stress transfer of >0.1 bar on most of the creeping segment of NTF, and also ˜0.1 bar on the NBF (Fig. 4a). The two peaks of cumulative scalar seismic moments of earthquakes are observed in these segments on NTF and NBF from the 2012 AVD until the 2019 TKC (Fig. 2b).

A cumulative positive normal stress transfer of >0.1 bar is obtained from AVD on most of the creeping segment of NTF (Fig. 4b). This additional positive normal stress to the regional stress may increase the effective normal stress on the creeping segment and change its rheology from partial creep to more stick-slip. The occurrence of two earthquakes on the proposed creep segment after the AVD which is also observed as a peak of the scalar seismic moment in Figure 2d confirms our suggestion.

On the NMF, two a wide peak of the cumulative scalar seismic moment was observed North of Urmieh Lake before AVD. While after the doublet, there is a peak of the cumulative scalar seismic moment in between of the previous wide peak suggesting that this part was partially locked, and has been excited by the doublet. Also, these seismic activities may be partly related to the relatively higher pore-fluid pressure provided by the Urmieh Lake on the NMF, or by the recent dramatic decrease of 90% of the water volume of the lake during years 1995 to 2013 (Schulz et al., 2020) that may reduce the effective normal stress on NMF, unclamp it, and excite it to slip.

5. Discussion

The seismicity of the NTF and NMF is investigated from documented historical earthquakes to November 2019 TKC earthquake. Many historical earthquakes are referred to NTF (Fig. 1a). The last two historical earthquakes of 1721 AD and 1780 AD cover all NTF segments. EHB catalog shows most of the seismic activity on the western termination of NTF. However, the GCMT catalog does not have any earthquake on the NTF.

The IRSC network earthquake catalog has improved from 2006 in terms of completeness and location accuracy. There are 512 earthquakes (45 of which have Ml>=2.5; Table S2) in the distance of 5 km from NTF and NMF for a period from 2006 until before AVD. These seismic activities are distributed along all segments of NTF and NMF unless the central segment of NTF that is situated North of SND and shows much less seismicity compared to its neighbor segments. Two remarkable peaks are observable in the cumulative scalar seismic moments of these earthquakes on both lobes of the central segment of NTF near SND (Figure 2b). A probable explanation for such behaviour is that the segment of NTF near SND is partially creeping. Djamour et al., (2011) and Rizza et al., (2013) reported a decrease in right-lateral surface deformation rate from West of BA (Longitude 47deg) to the East from 7mmy-1 to 5mmy-1. Su et al., (2017) remarked that the region near BA is affected by deep magmatic activities of SND. This segment is close to the thermal areas (hot springs) near BA reported by Ghalamghash et al. (2019). Tomography studies by Rezaeifar et al., (2016) and Bavali et al., (2016) revealed a heterogeneous structure in this region with high and low-velocity anomalies. A low-velocity region has obtained beneath SND at depths deeper than 8 km that extends until the NTF by Bavali et al., (2016) (Fig. 5). However, at shallower depths, a relatively high-velocity anomaly obtained by Rezaeifar et al., (2016), and interpreted as cooled magmatic rocks of SND. The observed thermal activities near BA area are probably due to the existence of some dyke-like branches of the SND deep magma chamber in that area that was also suggested by Ghalamghash et al. (2019) as many young craters with dacitic to rhyolitic parasitic cones of magma of neo-Sahand were observed toward NNE of SND near BA (see Fig. 3). The other explanation will be the possible aid of NTF fractured area which is extended down to the depth of 20 km, in bringing heat to the surface. The existing heat increases the pore-fluid pressure in the fault area and unclamps this segment of NTF, facilitating its creep.

However, this segment of NTF was ruptured as a part of the 1721 AD M7.6 earthquake. Harris, (2017) mentioned that the creeping segments are also potential to rupture in M~6.8 earthquakes, and they usually rupture together with their nearby segments (i.e. Van den Ende et al., 2020). Dynamic weakening is the probable mechanism for rupture of such fault segments (i.e. Noda & Lapusta, 2013). The same mechanism may have happened during the 1721 AD earthquake, and that is most likely the reason for segmentation of NTF during 1721 AD and 1780 AD historical earthquakes.

The effect of raise of pore-fluid pressure in facilitating the fault creep/slip is widely observed and reported mostly for Strike-slip faulting mechanism (e.g. Avouac, 2015, Floyd et al., 2016, Goebel et al., 2017, Scuderi et al., 2017, Michel et al., 2018, Johann et al., 2018, Eaton & Schultz, 2018, Zhu et al., 2020, Momeni & Madariaga, 2020).

A slip model is estimated for the creeping segment of NTF from 1721 AD until before the 2012 AVD considering that half of the 7 mmy-1 right-lateral deformation rate obtained by Djamour et al., (2011) and Rizza et al., (2013) was happening in creep mode. This creep has occurred at the longitudes between 46.55deg E to 46.85deg E and with a locking depth of 20 km. Having a maximum cumulative slip of 1.02m, the obtained cumulative scalar seismic moment is 2.0 * e+19 Nm equal to Mw6.8 (for the fully creep mode, this value raises to 4.0 * e+19 Nm equal to Mw7.0). This also remarks that the other segments of NTF have a considerable amount of accumulated tectonic stress.

The creeping segment of NTF transferred positive Coulomb stress field of >4 bar on the neighbor segments, and brought them closer to failure (Fig. 3b). That is confirmed by the observation of two peaks of cumulative scalar seismic moments on both lobes of the creeping segment. These earthquakes can be considered as aftershocks of the creep event. Aftershocks surrounding a slip model is a consistent feature of large earthquakes (see Henry & Das, 2002).

The 3D stress field produced by this creep source on AVD is computed. The estimated slip model for the creeping segment can transfer positive Coulomb stress of >1 bar on the AVD and trigger them (Fig. 6). After the AVD until November 2019, one peak of the cumulative scalar seismic moment is observed for earthquakes occurred in 5 km distance from NTF, and that is in the middle of the central NTF. There is also one peak on the NMF. Observation of seismic activity on the previously creeping segment of NTF and absence of two peaks of cumulative scalar seismic moments on both lobes of that segment suggest a change in its rheology from creep to stick-slip after AVD. This change is probably due to the positive static normal stress field of >0.1 bar that was transferred from AVD on half of the creeping segment of NTF. Also, Momeni et al., (2019) compute the stress field by AVD on NTF and NMF and reported transfer of positive Coulomb stress of >0.1 bar on the central segment of NTF as well as NMF. For the NMF, two relatively small peaks of cumulative scalar seismic moment release are observed before the AVD (Fig. 2b). After AVD, one big peak is observed in between the two previous peaks suggesting that this part of NMF was partially locked, and triggered by the 2012 AVD.

Seismic quiescence of the creeping segment of NTF near SND from 2006 together with the observed magmatic activities in that area proposes a strong relation between the volcanic activity of SND and frictional properties of that segment of NTF. Compared to the central NTF, the western segment that is closer to the Tabriz city shows higher seismic activity. Also, the Eastern segment shows considerable seismic activity which highlights its importance as another potential segment of the NTF for future large earthquakes.

The smooth geometry of the central and western segments of NTF may facilitate the rupture expansion on them. However, low seismic coupling in the creeping central NTF may act as a barrier and stop ruptures from expansion toward the western segment.

The suggested 20km thick seismogenic layer for NTF (Djamour et al., 2011; Moradi et al. 2011), highlights its potential for the production of large earthquakes and with low-frequency seismic energy contents that can reach to Tabriz city with less damped energy and affect the tall buildings.

6. Conclusion

I infer a seismic quiescence in the central segment of the NTF, North of SND from 2006 until August 2012 AVD. While the two eastern and western segments of NTF show much higher seismicity with two remarkable peaks of cumulative scalar seismic moments on both lobes of the central segment near SND. The existing heat by the SND magma chamber near the fractured area of central NTF raises the pore-fluid pressure and decreases the effective normal stress there, consequently unclamp the fault, and facilitate the right-lateral creep. An Mw6.8 half-creep slip model is suggested for this segment considering half of 7 mmy-1 constant geodetic deformation rate on it since the 1721 AD historical earthquake.

The creeping segment is situated in almost the same longitude range to the 2012 AVD and transferred positive Coulomb stress fields of >1 bar on them. This segment also transferred >4 bar of positive Coulomb stress on its neighbor segments, where the two peaks of cumulative seismic moments were observed. Some of the right-lateral deformation stresses on central NTF transferred to the North and released during the 2012 AVD on the Ahar-Varzaghan complex fault system (Fig. 6).

After the AVD until TKC, two new peaks of the cumulative scalar seismic moment have observed for earthquakes that occurred on NTF and NMF. One is exactly in the middle of the previously creeping central segment of NTF, consistent to the obtained transfer of positive normal and Coulomb stresses on this segment by AVD (i.e. Momeni et al., 2019). The transferred stress changed the rheology of the creeping segment from mostly creeping to temporary stick-slip.

The other peak of the cumulative scalar seismic moment is on the NMF North of Urmieh Lake, and, may be due to the existing pore-fluid pressure or a recent dramatic decline in the water level of the lake over the past two decades (90% decrease in its volume has happened during 1995 to 2013; Schulz et al., 2020) that both reduce the effective normal stress on NMF, unclamp it, and facilitate slip on it (e.g. Saar & Manga, 2003).The two peaks of cumulative scalar seismic moments observed before AVD on the western and eastern lobes of the creep segment of NTF near SND were disappeared after AVD until November 2019 TKC, suggesting a change in seismic activity of NTF along its segments by the transferred stress fields produced by AVD, at least for the first 8 years. This change is probably temporary and NTF will return to continue its creep behaviour in the central segment near SND.

In terms of rupture dynamics, the two highly stressed neighbor segments of NTF are prone to nucleate earthquakes (e.g. Vadacca et al., 2020). If an earthquake nucleates on the stressed lobes of the creeping segment and its rupture grow toward the West, it will cause a strong directivity effect for that earthquake toward Tabriz city. However, the creeping segment may work as a barrier and probably does not allow NTF to rupture in both Central and Western segments in one larger earthquake.

The change in seismic activity on the different segments of NTF and having mix behaviour of lock and creep deformation on them raise the seismic hazard in the region, especially for the Tabriz city that currently host > 2 million people. I suggest continuous monitoring of seismicity along NTF will help to understand the rheological behaviours of segments of this mature fault system, with a concentration on the central and western segments that did not rupture in large events since the 1721 AD and 1780 AD historical earthquakes.

7. Data and Resources

The earthquakes data are available through the Iranian Seismological Center (IRSC) network website (http://irsc.ut.ac.ir). The earthquake focal mechanisms in Figure 1b are from the GCMT catalog (http://www.globalcmt.org/CMTsearch.html last access on August, 2020). The supplementary data includes velocity model of the area and earthquakes hypocenters information.

8. Acknowledgements

This research did not receive any specific grant from funding agencies in the public, commercial, or not-for-profit sectors. I thank IRSC and IIEES networks for providing the seismic data. Figures plotted using Generic Mapping Tools (GMT) (http://gmt.soest.hawaii.edu/), Paraview software (https://www.paraview.org), and personal codes in Matlab environment (https://www.mathworks.com).

9. References

Ambraseys, N.N. & Melville, C.P., 1982. A History of Persian Earthquakes, Cambridge Univ. Press. https://doi.org/10.1016/j.jseaes.2008.08.001

Avouac, J.P., 2015. From Geodetic Imaging of Seismic and Aseismic Fault Slip to Dynamic Modeling of the Seismic Cycle, Annu. Rev. Earth Planet. Sci. 2015. 43:233–71, doi: 10.1146/annurev-earth-060614-105302.

Aziz Zanjani, A., Ghods, A., Sobouti, F., Bergman, E., Mortezanejad, G., Priestley, K., Madanipour, S., Rezaeian, M., 2013. Seismicity in the western coast of the South Caspian Basin and the Talesh Mountains. Geophys. J. Int. 194, 799–814. https://doi.org/10.1093/gji/ggt299

Bavali, K., Motaghi, K., Sobouti, F., Ghods, A., Abbasi, M., Priestley, K., Mortezanejad, G., Rezaeian, M., 2016. Lithospheric structure beneath NW Iran using regional and teleseismic travel-time tomography, Physics of the Earth and Planetary Interiors 253, 97–107. http://dx.doi.org/10.1016/j.pepi.2016.02.006

Berberian, M., Arshadi, S., 1976. On the evidence of the youngest activity of the North Tabriz Fault and the seismicity of Tabriz city. Geol. Surv. Iran Rep. 39, 397–418.

Berberian, M., 1997, Seismic sources of the Transcaucasian historical earthquakes. In S. Giardini and Balassanian, S. (Eds.), Historical and prehistorical earthquakes in the Caucasus. Kluwer Academic Publishing, Dordrecht, Netherlands, pp. 233–311.

Berberian, M. & Yeats, R.S., 1999. Patterns of historical earthquake rupture in the Iranian Plateau. Bulletin of the Seismological Society of America **89** , 120–139.

Berberian, M. & Yeats, R.S., 2001. Contribution of archaeological data to studies of earthquake history in the Iranian Plateau. Journal of Structural Geology **23** , 563–584.

Copley, A., Faridi, M., Ghorashi, M., Hollingsworth, J., Jackson, J., Nazari, H., Oveisi, B., Talebian, M., 2013. The 2012 August 11 Ahar earthquakes: consequences for tectonics and earthquake hazard in the Turkish-Iranian plateau. Geophys. J. Int. 196, 15–21. http://dx.doi.org/10.1093/gji/ggt379

Djamour, Y., Vernant, P., Nankali, H.R. & Tavakoli, F., 2011. NW Iran eastern Turkey present-dat kinematics: results from the Iranian permanent GPS network, Earth planet. Sci. Lett., 307, 27–34. http://dx.doi.org/10.1016/j.epsl.2011.04.029

Donner, S., Ghods, A., Krauger, F., Rossler, D., Landgraf, A. & Ballato, P., 2015. The Ahar-Varzeghan earthquake doublet (Mw 6.4 and 6.2) of 11 August 2012: regional seismic moment tensors and a seismotectonic interpretation, Bull. seism. Soc. Am., 105, doi:10.1785/0120140042.

Eaton, D.W., & Schultz, R., 2018. Increased likelihood of induced seismicity in highly overpressured shale formations, Geophysical Journal International, 214(1), 751–757, https://doi.org/10.1093/gji/ggy167.

Engdahl, E.R.; Jackson, J.A.; Myers, S.C.; Bergman, E.A.; Priestley, K. Relocation and assessment of seismicity in the Iran region. Geophys. J. Int. 2006, 167, 761–778. http://dx.doi.org/10.1111/j.1365-246X.2006.03127.x

Floyd, M.A., et al., 2016. Spatial variations in fault friction related to lithology from rupture and afterslip of the 2014 South Napa, California, earthquake, Geophys. Res. Lett., 43, doi:10.1002/2016GL069428.

Ghalamghash, J., Schmitt, A.K., Chaharlang, R., 2019. Age and compositional evolution of Sahand volcano in the context of post-collisional magmatism in northwestern Iran: Evidence for time-transgressive magmatism away from the collisional suture, Lithos 344–345 (2019) 265–279, https://doi.org/10.1016/j.lithos.2019.06.031.

Ghods, A., Shabanian, E., Bergman, E., Faridi, F., Donner, S., Mortezanejad, G., Aziz- Zanjani, A., 2015. The Varzaghan-Ahar, Iran, Earthquake Doublet 1 (Mw 6.4, 6.2): implications for the geodynamics of northwest Iran. Geophys. J. Int. 203, 522–540. http://dx.doi.org/10.1093/gji/ggv306

Goebel, T.H.W., Weingarten, M., Chen, X., Haffener, J., Brodesky, E.E., 2017. The 2016 Mw5.1 Fairview, Oklahoma earthquakes: Evidence for long-range poroelastic triggering at >40 km from fluid disposal wells, Earth and Planetary Science Letters, 472, 50-61. https://doi.org/10.1016/j.epsl.2017.05.011

Harris, R. A. (2017), Large earthquakes and creeping faults, Rev. Geophys., 55, 169-198, doi:10.1002/2016RG000539.

Henry, C., & S. Das, 2002. The Mw 8.2 17 February 1996 Biak, Indonesia, earthquake: Rupture history, aftershocks, and fault plane properties, J. Geophys. Res., **107** (B11), 2312, doi: 10.1029/2001JB796.

Hessami Azar, K., Pantosti, D., Tabassi, H., Shabanian, E., Abbasi, M.R., Feghhi, K., Solaymani, S., 2003. Paleoearthquakes and slip rates of the North Tabriz Fault, NW Iran: preliminary results. Ann. Geophys. 46, 903–915. DOI: https://doi.org/10.4401/ag-3461

Jackson, J., 1992. Partitioning of strike-slip and convergent motion between Eurasia and Arabia in Eastern Turkey and the Caucasus. J. Geophys. Res. 97, 12471–12479. https://doi.org/10.1029/92JB00944

Jackson, J., Priestley, K., Berberian, M., 2002. Active tectonics of the South Caspian Basin. Geophys. J. Int. 148, 214–245. https://doi.org/10.1046/j.1365-246X.2002.01588.x

Johann, L., Shapiro, S.A. & Dinske, C., 2018. The surge of earthquakes in Central Oklahoma has features of reservoir-induced seismicity. Sci Rep 8, 11505. https://doi.org/10.1038/s41598-018-29883-9.

Kagan, Y. Y., and Jackson, D. D., 1991, Long-term earthquake clustering, Geophys. J. Int., 104, 117–133. https://doi.org/10.1111/j.1365-246X.1991.tb02498.x

Karakhanian, A., Jrbashyan, R., Trifonov, V., Philip, H., Avagyan, A., Hessami, K., Jamali, Bayraktutan, F. M., Bagdassarian, H., Arakelian, S., Davtyan V., and Adilkhanyan, A., 2004, Active faulting and natural hazards in Armenia, eastern Turkey and Northern Iran, Tectonophysics, 380, 189–219. https://doi.org/10.1016/j.tecto.2003.09.020

Khoshmanesh, M., Shirzaei, M., 2018. Episodic creep events on the San Andreas Fault caused by pore pressure variations, Nat. Geosci. https://doi.org/10.1038/s41561-018-0160-2

Masson, F., Djamour, Y., Van Gorp, S., Chery, J., Tatar, M., Tavakoli, F., Nankali, H. & Vernant, P., 2006. Extension in NW Iran driven by the motion of the South Caspian Basin, Earth planet. Sci. Lett., 252, 180–188. https://doi.org/10.1016/j.epsl.2006.09.038

Michel, S., Avouac, J.P., Jolivet, R., and Wang, L., 2018. Seismic and Aseismic Moment Budget and Implication for the Seismic Potential of the Parkfield Segment of the San Andreas Fault, Bulletin of the Seismological Society of America, Vol. 108, No. 1, pp. 19–38, Doi: 10.1785/0120160290.

McClusky, S., et al., 2000. Global positioning system constraints on plate kinematics and dynamics in the eastern Mediterranean and Caucasus. J. Geophys. Res. 105, 5695–5719. https://doi.org/10.1029/1999JB900351

Momeni, S.M., Tatar, M., 2018. Mainshocks/aftershocks study of the August 2012 earthquake doublet on Ahar-Varzaghan complex fault system (NW Iran). Physics of the Earth and Planetary Interiors, **283** , 67-81. https://doi.org/10.1016/j.pepi.2018.08.001

Momeni, S.M., Aoudia, A., Tatar, M., Twardzik, C. & Madariaga, R., 2019. Kinematics of the 2012 Ahar–Varzaghan complex earthquake doublet (M_w6.5 and M_w6.3), *Geophysical Journal International* , **217** , 2097–2124, https://doi.org/10.1093/gji/ggz100

Momeni, S.M., Madariaga, R., 2020. Long-term induced seismicity on the Mosha fault by Damavand Volcano, N-Iran, Implications on the seismic hazard of Tehran metropolis, under review in SRL.

Moradi, A.S., Hatzfeld, D. & Tatar, M., 2011. Microseismicity and seismotectonics of the North Tabriz Fault (Iran), Tectonophysics, 506, 22–30. https://doi.org/10.1016/j.tecto.2011.04.008

Noda, H., & Lapusta, N., 2013, Stable creeping fault segments can become destructive as a result of dynamic weakening, NATURE,**493** , 518-521, doi:10.1038/nature11703

Schulz, S., Darehshouri, S., Hassanzadeh, E. et al. 2020. Climate change or irrigated agriculture – what drives the water level decline of Lake Urmia. Sci Rep 10, 236. https://doi.org/10.1038/s41598-019-57150-y.

Su, Z., Wang, E., Hu, J., Talebian, M. & Karimzadeh, S., (2017). Quantifying the Termination Mechanism Along the North Tabriz-North Mishu Fault Zone of Northwestern Iran via Small Baseline PS-InSAR and GPS Decomposition. IEEE Journal of Selected Topics in Applied Earth Observations and Remote Sensing, vol. 10, no. 1, pp. 130-144, doi: 10.1109/JSTARS.2016.2586742.

Reilinger, R., et al., 2006. GPS constraints on continental deformation in the Africa- Arabia-Eurasia continental collision zone and implications for the dynamics of plate interactions. J. Geophys. Res. 111, B05411. https://doi.org/10.1029/2005JB004051.

Rezaeifar, M., Kissling, E., Shomali, Z.H. & Shahpasand-Zadeh, M., 2016. 3D crustal structure of the northwest Alborz region (Iran) from local earthquake tomography. Swiss J. Geosci., 1–12, Springer International Publishing. doi:10.1007/s00015-016-0219-2

Rizza, M., Vernant, P., Ritz, J., Peyrat, M., Nankali, H., Nazari, H., Djamour, Y., Salamati, R., Tavakoli, F., Chery, J., Mahan, S., Masson, F., 2013. Morphotectonic and geodetic evidence for a constant slip-rate over the last 45 kyr along the Tabriz fault (Iran). Geophys. J. Int. 193, 1083–1094. https://doi.org/10.1093/gji/ggt041

Ruiz, S., & Madariaga, R., 2013. Kinematic and dynamic inversion of the 2008 northern Iwate earthquake, Bull. Seismol. Soc. Am.,**103** (2A), 694–708, Doi: 10.1785/0120120056.

Saar, M.O., Manga, M., 2003. Seismicity induced by seasonal groundwater recharge at Mt. Hood, Oregon, Earth and Planetary Science Letters, 214, 605-618. https://doi.org/10.1016/S0012-821X(03)00418-7

Scuderi, M.M., Collettini, C., Marone, C., 2017. Frictional stability and earthquake triggering during fluid pressure stimulation of an experimental fault, Earth and Planetary Science Letters, **477** , 84-96. https://doi.org/10.1016/j.epsl.2017.08.009

Solaymani Azad, S., Philip, H., Dominguez, S., Hessami Azar, K., Shahpasandzadeh, M., Foroutan, M., Tabassi, H., Lamothe, M., 2015. Paleoseismological and morphological evidence of slip rate variations along the North Tabriz fault (NW Iran). Tectonophysics, 640–641, 20-38. https://doi.org/10.1016/j.tecto.2014.11.010

Van den Ende, M.P.A., Chen, J., Ampuero J.P. & Niemeijer A.R., 2020. Rheological Transitions Facilitate Fault-Spanning Ruptures on Seismically Active and Creeping Faults, Journal of Geophysical Research: Solid

Earth Volume 125, Issue 8, https://doi.org/10.1029/2019JB019328

Vadacca, L., 2020, The Altotiberina Low-Angle Normal Fault (Italy) Can Fail in Moderate-Magnitude Earthquakes as a Result of Stress Transfer from Stable Creeping Fault Area, Geosciences, 10, 144; doi:10.3390/geosciences10040144.

Valerio, E., Manzo, M., Casu, F., Convertito, V., De Luca, C., Manunta, M., Monterroso, F., Lanari, R. & De Novellis, V., 2020. Seismogenic Source Model of the 2019, Mw 5.9, East-Azerbaijan Earthquake (NW Iran) through the Inversion of Sentinel-1 DInSAR Measurements, Remote Sens., 12, 1346; doi:10.3390/rs12081346.

Vernant, Ph., et al., 2004. Contemporary crustal deformation and plate kinematics in Middle East constrained by GPS measurements in Iran and northern Oman. Geophys. J. Int. 157, 381–398.

Wang, R., Martin, F.L., Roth, F., (2003). Computation of deformation induced by earthquakes in a multi-layered elastic crust—FORTRAN programs EDGRN/EDCM, Computers & Geosciences 29, 195–207, 2003.

Zamani, B., Masson, F., 2014. Recent tectonics of East (Iranian) Azerbaijan from stress state reconstructions. Tectonophysics 611, 61–82.

Zhu, W., Allison, K.L., Dunham, E.M., Yang, Y., 2020. Fault Valving and Pore Pressure Evolution in Simulations of Earthquake Sequences and Aseismic Slip, Computational Physics, https://arxiv.org/abs/2001.03852.

Mailing address:

Seyyedmaalek Momeni

EPFL Geo-Energy Lab – Gaznat Chair on Geo-Energy, EPFL-ENAC-IIC-GEL, Station 18, CH-1015, Lausanne, Switzerland.

Figure Captions:

Figure 1 . (**a**) Seismotectonics of the study region. Stars show the 2012 AVD hypocenter locations, and the related focal mechanisms are by Momeni & Tatar, (2018). Faults are in lines. Vectors are geodetic surface deformation rates by Masson et al., (2006), fixing the central Iran block. Hexagons are historical earthquakes (Ambraseys & Melvile, 1982; Berberian & Yeats, 1999, 2001). Circles are instrumental earthquakes by Engdahl et al. (2006). Dashed ellipses show affected regions by the 1593, 1721, 1780, and 1786 historical earthquakes. Fault names are: ASF: Astaneh, WAF: West Alborz, SQF: South Qoshadagh, GCF: Goshachay, NBF: North Bozkosh, SBF: South Bozkosh, NMF: North Mishu, SMF: South Mishu, MGF: Maraghe, NKH: Nakhjavan, KHF: Khajeh, and NHF: Nehram. NTF is in thick solid line. (**b**) Circles: Seismicity recorded in IRSC network from 2006 until before the AVD. Colors represent hypocentral depths. Faults are the same as (a). Focal mechanisms with label are from the GCMT catalog until August 2020. Those labeled M6.1 ARD, M6.5 AVD1, M6.3 AVD2, and M5.9 TKC are from the 1997 Ardebil, 2012 AVD doublet and 2019 Mw5.9 Torkamanchay earthquakes. Triangles are the Tabriz permanent seismic sub-network stations belong to IRSC.

Figure 2 . Seismicity along NTF and NMF. (**a**): black circles are the earthquakes from 2006 to before the 2012 AVD and white circles are the earthquakes that occurred after 2012 AVD until 2019 TKC. Ellipse is the estimated cumulative slip model for the creeping segment of NTF near SND from 1721 AD historical earthquake until AVD. The dashed circle is the thermal area (after Ghalamghash et al, 2019). (**b**) up: histogram showing seismicity selected in distance of 5 km from NTF and NMF shown in (a). NMF stands for North Mishu Fault. down: Diagram of cumulative scalar seismic moments along NTF and NMF.

Figure 3 . Transferred Coulomb stress field from the creeping segment of NTF on the (**a**) AVD ruptures and (**b**) the Western and Eastern segments of the creep segment of NTF, where high seismic activity was observed. The shown Coulomb stress fields are for the depth of 6 km. Circles along NTF are earthquakes from 2006 until AVD. The rest are early aftershocks of the AVD (IRSC). Dashed circle is the thermal area by Ghalamghash et al., (2019). Solid large circle shows the area of neo-Sahand young craters near Bostan Abad (BA). Dashed line marked A is the position of vertical cross sections shown in Figures 5 and 6.

Figure 4 . (**a**): Transferred Coulomb stress fields from AVD ruptures on NTF (up: EV#1, down: EV#2). (**b**): Transferred Normal stress fields from AVD ruptures on NTF (up: EV#1, down: EV#2). The shown stress fields are for the depth of 10 km.

Figure 5. Schematic plot illustrating the relation between SND magmatic activity, NTF creeping segment, and AVD ruptures (marked AV#1 & AV#2). Low and high velocity areas are from Bavali et al., (2016), Rezaeifar et al., (2016), and Ghalamghash et al, (2019) studies. Stars are the 11 August 2012 M6.5&M6.3 mainshocks centroids. Thick dashed line is the NTF. Horizontal dashed lines are crustal velocity layers from Momeni & Tatar, (2018).

Figure 6. Graphic illustration of triggering of the 2012 AVD by the transfer of Coulomb stress field produced by the central NTF creeping segment. Stars are the mainshocks hypocenters. Rupture models are from Momeni et al., (2019). Horizontal dashed lines are crustal velocity layers from Momeni & Tatar, (2018).

Figures:

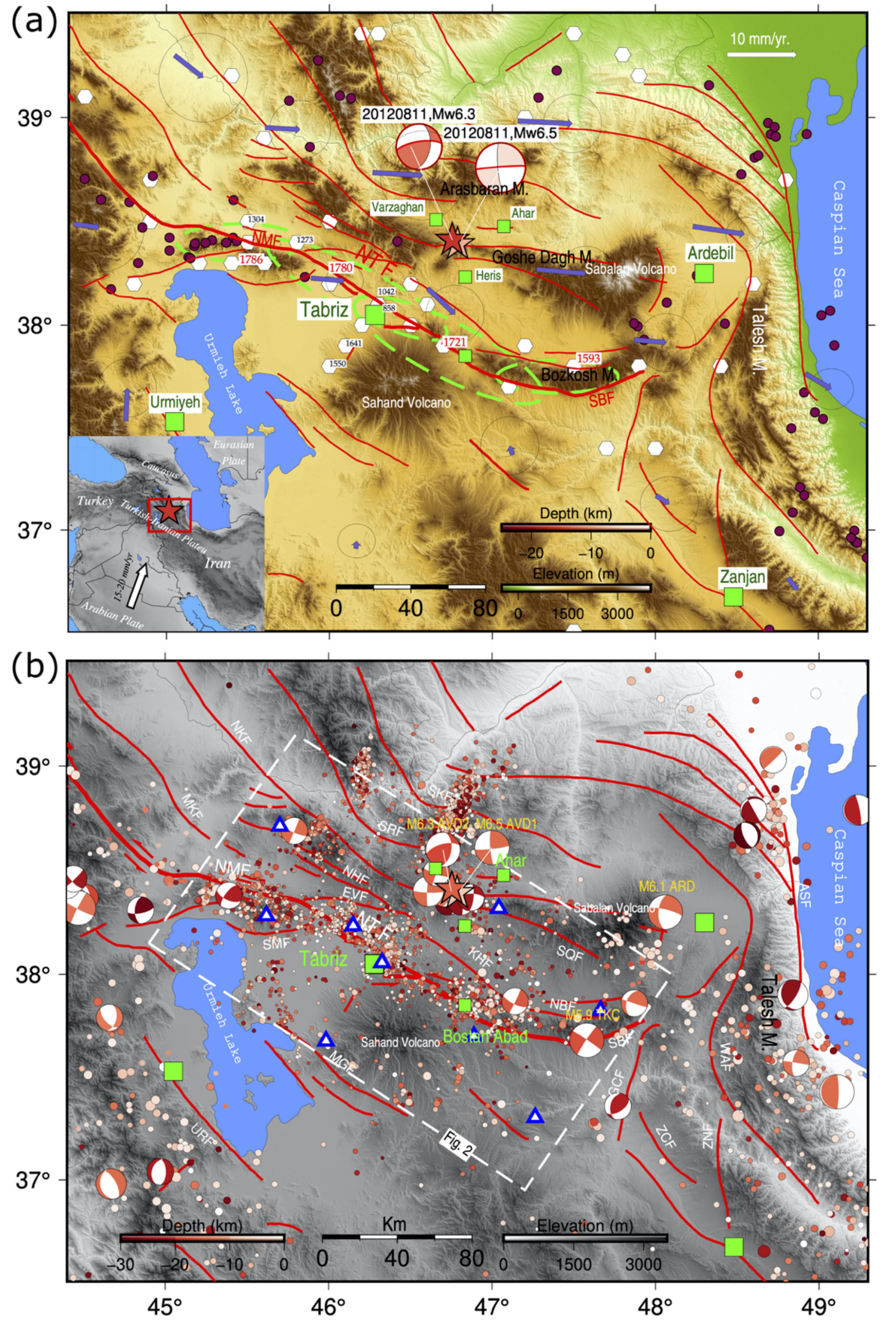

Figure 1 . **(a)** Seismotectonics of the study region.**(b)** Seismicity recorded in IRSC network from 2006 until before the AVD.

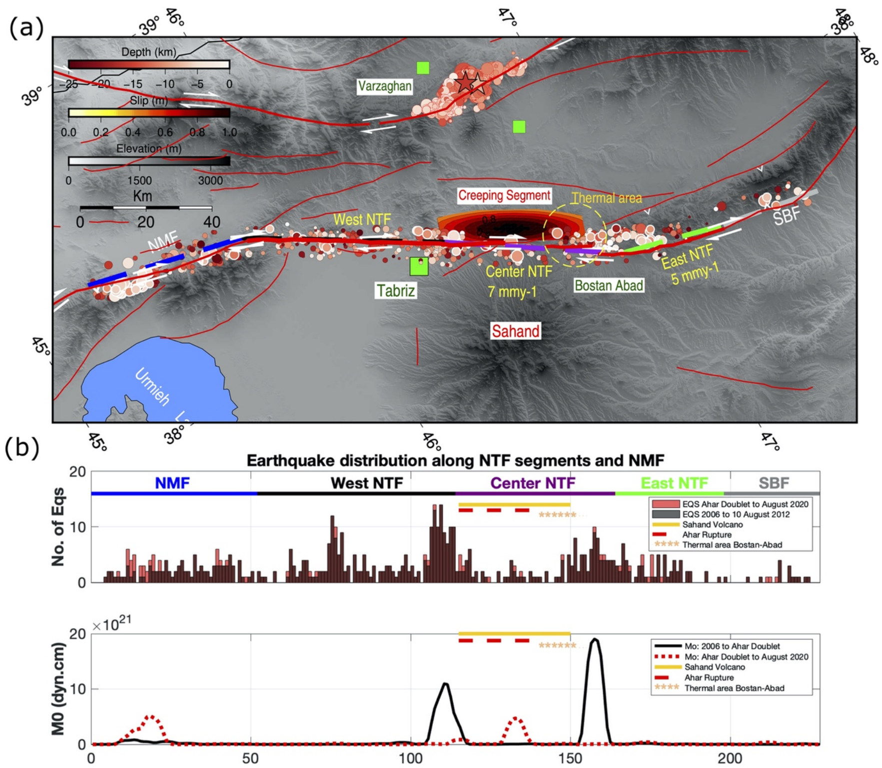

Figure 2 . **(a)** Seismicity along NTF and NMF.**(b)** Histograms of earthquake distribution along NTF and NMF.

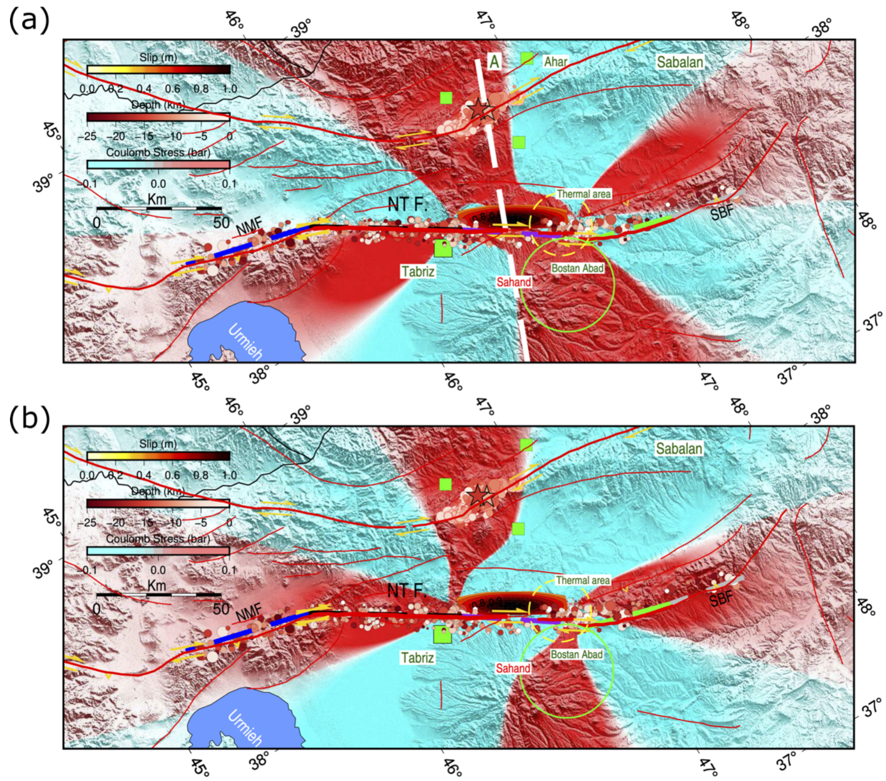

Figure 3 . Transferred Coulomb stress field from the creeping segment of NTF. **(a)** on the AVD ruptures and**(b)** on the Western and Eastern segments of the creeping segment.

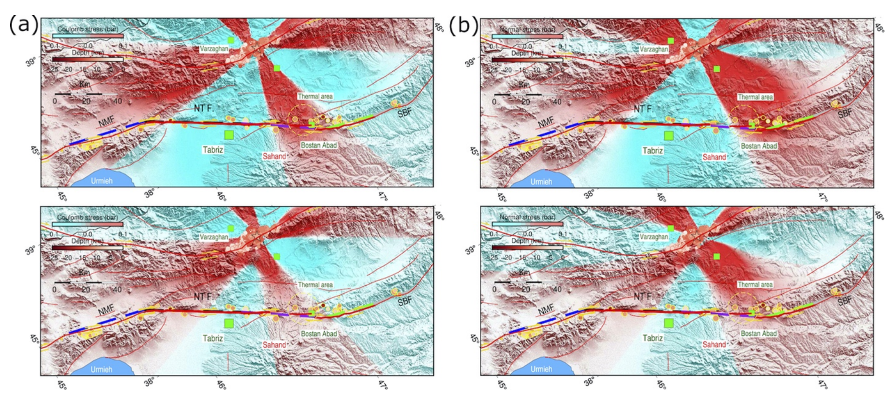

Figure 4 . Transferred **(a)** Coulomb and**(b)** Normal stress fields from AVD ruptures on NTF.

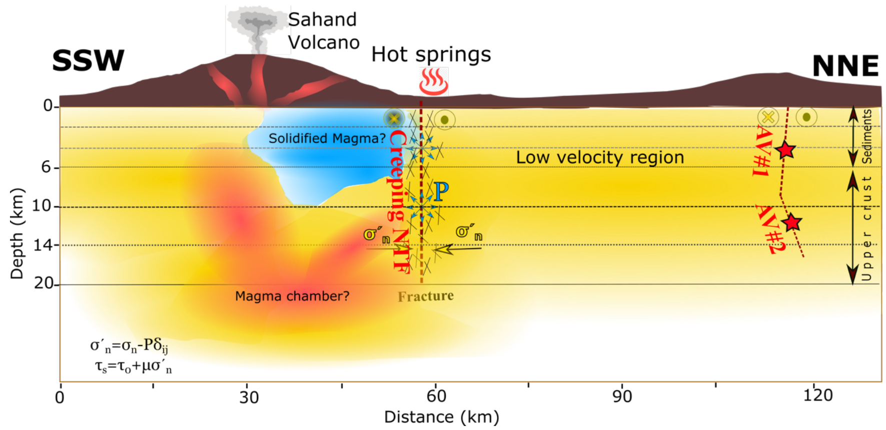

Figure 5 . Schematic plot illustrating the relation between SND magmatic activity, NTF creeping segment, and AVD ruptures.

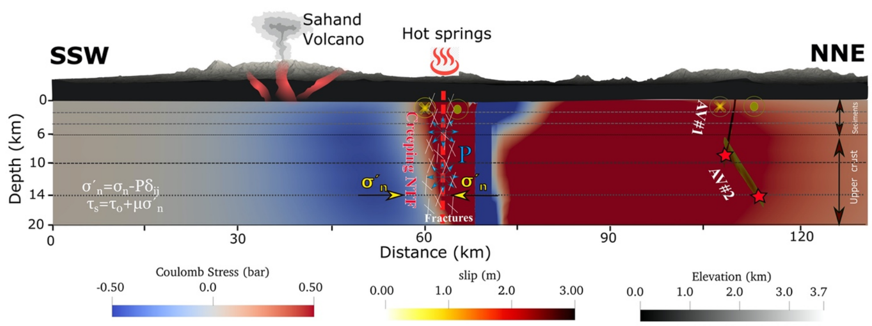

Figure 6 . Graphic illustration of triggering of the 2012 AVD by the transfer of Coulomb stress field produced by the central NTF creeping segment.

Electronic Supplement

Tables:

Table S1. Velocity model of the NW Iran by Momeni & Tatar, (2018).

Depth of layer top	Vp	Vs
-3	4.58	2.44
2	5.65	3.11
4	5.92	3.34
6	6.20	3.53
10	6.35	3.63
14	6.52	3.71
46	8.10	4.63

Table S2. Earthquakes with Ml>=2.5 along the North Tabriz fault segments and NMF and SBF from 2006 until before the August 2012 Ahar-Varzaghan earthquake doublet (Mw6.5&6.3) (IRSC).

	Longitude	Latitude	Year	Month	Day	Magnitude	Depth	Hour	Minute
Central NTF	46.56	37.95	2007	10	4	2.7	12.80	3	2
	46.43	38.09	2007	12	1	4.5	7.4	18	45
	46.64	37.94	2008	3	24	3.1	11.8	9	44
	46.42	38.10	2008	4	7	3.2	11.4	2	48
	46.42	38.09	2008	5	10	3.3	15.1	16	15
	46.57	37.96	2009	6	13	2.7	15.5	23	21
	46.82	37.87	2009	10	12	2.7	9.8	20	55
	46.84	37.86	2010	2	2	3.6	5.0	10	5
	46.84	37.83	2010	2	2	3.4	2.1	10	15
	46.84	37.86	2010	2	2	4.6	5.0	10	16
	46.83	37.84	2010	2	2	3.8	5.0	11	26
Eastern NTF	47.21	37.72	2006	2	2	2.9	8.4	19	49
	46.99	37.81	2007	5	26	2.5	8.4	22	1
	47	37.73	2007	6	21	2.7	3.5	16	27
	46.97	37.82	2008	1	28	2.8	5.4	13	38
	47.13	37.73	2008	4	19	3.1	18	13	36
	46.88	37.84	2010	2	2	3.0	11.6	13	23
	47.04	37.77	2011	10	18	2.9	1.7	21	4
Western NTF	46.22	38.20	2006	1	8	3.1	4.0	17	19
	46.34	38.07	2008	1	22	2.5	10	8	55
	46.34	38.14	2008	6	1	2.6	13.50	2	17
	46.18	38.16	2008	6	26	2.6	16.20	16	34
	46.20	38.15	2008	6	26	2.6	14.70	16	39
	46.18	38.16	2008	6	26	3.1	16.70	17	6
	46.18	38.16	2008	6	26	2.7	15.80	17	8
	46.35	38.13	2008	7	28	2.9	17.20	7	13
	46.10	38.23	2009	2	13	2.6	5.1	4	0
	46.39	38.11	2009	8	5	2.6	10.40	22	15
	45.93	38.29	2010	1	4	2.6	10	7	38
	46.34	38.12	2011	1	29	3	14.80	7	29
	46.36	38.10	2012	5	4	2.6	7.8	21	48
NMF	45.47	38.41	2006	8	12	3.6	13.60	7	2
	45.35	38.49	2007	7	8	2.6	15.80	22	49
	45.38	38.40	2008	4	22	3.7	9	19	53
	45.74	38.34	2008	9	6	2.6	3	11	8
	45.41	38.47	2009	4	24	3.6	3.8	18	28
	45.45	38.39	2011	8	19	2.6	19.8	4	31
	45.69	38.36	2012	2	5	2.9	23.6	22	15
	45.57	38.43	2012	4	29	3.2	8	0	16
	45.55	38.42	2012	4	29	3	11.20	0	22
SBF	47.55	37.64	2008	6	12	2.5	10	3	19
	47.29	37.75	2010	7	14	2.9	18	16	46
	47.54	37.68	2010	10	23	2.7	4.10	17	59
	47.55	37.66	2011	6	6	3.1	0.70	12	23
	47.55	37.64	2008	6	12	2.5	10	3	19

Table S3. Earthquakes with Ml>=2.5 along the North Tabriz fault segments and NMF and SBF from the August 2012 Ahar-Varzaghan earthquake doublet until the November 2019 Mw5.9 Torkamanchay earthquake (IRSC).

	Longitude	Latitude	Year	Month	Day	Magnitude	Depth	Hour	Minute
Central NTF	46.47	38.06	2012	12	13	2.7	18	0	29
	46.75	37.93	2012	12	16	3.2	10	10	41
	46.42	38.09	2014	3	9	3.6	7.4	6	34
	46.59	37.93	2015	1	19	3.8	9.5	11	53
	46.84	37.87	2015	12	2	2.8	8	0	31
	46.52	38.00	2016	1	27	3.0	14.7	20	31
	46.43	38.04	2016	6	27	2.5	19.6	18	38
	46.42	38.03	2017	1	5	2.6	5.7	4	33
	46.43	38.06	2018	12	12	3.5	6	5	56
	46.44	38.07	2018	12	21	3.6	5	9	39
	46.60	37.98	2019	8	16	4.2	8.9	10	55
Eastern NTF	47.03	37.80	2013	2	8	2.6	10	19	25
	46.95	37.82	2013	2	12	2.5	5.1	8	11
	47.05	37.76	2014	2	11	2.7	5.4	10	18
	47.04	37.77	2014	8	19	2.5	10	5	43
	47.02	37.78	2014	9	8	2.8	10	16	53
	47.04	37.80	2018	6	1	2.5	10	0	8
	46.99	37.79	2018	11	24	3.3	8.6	17	22
	47.01	37.78	2018	11	25	2.5	10	9	46
	47.00	37.78	2018	11	26	3.3	6	20	9
	46.99	37.79	2018	11	27	2.7	6	11	33
Western NTF	45.89	38.29	2013	10	12	2.9	6	5	48
	45.90	38.35	2015	2	5	2.5	6.9	7	40
	46.38	38.13	2015	4	4	2.8	10	21	24
	45.97	38.30	2016	10	28	2.7	19.3	9	18
	46.31	38.07	2016	11	14	3.6	7.6	3	35
	45.98	38.28	2016	12	29	2.6	10	8	36
	46.34	38.12	2017	3	31	2.7	10	20	4
	46.32	38.07	2017	6	23	2.6	8	4	35
	46.04	38.23	2018	1	22	3.2	8.4	15	59
	46.04	38.23	2018	1	22	2.9	9.4	16	14
	46.34	38.14	2018	5	6	2.7	9.4	8	33
	46.36	38.11	2018	6	22	2.9	10	17	5
	46.34	38.13	2019	5	8	2.9	8.9	22	57
NMF	45.36	38.43	2013	4	18	4.9	6.1	10	39
	45.34	38.41	2013	4	18	3	10.2	10	53
	45.35	38.42	2013	4	18	2.9	12	11	32
	45.38	38.41	2013	4	18	3.9	6.4	11	40
	45.33	38.42	2013	4	18	2.6	30.3	13	30
	45.39	38.40	2013	4	29	2.6	12.6	14	36
	45.41	38.40	2013	6	28	4.2	5.30	5	13
	45.46	38.45	2014	3	12	2.6	10.8	10	28
	45.60	38.43	2014	5	13	2.5	9.8	3	59
	45.30	38.44	2015	4	10	2.5	10	19	17
	45.75	38.34	2015	12	31	3	11.8	22	31
	45.65	38.37	2016	2	15	2.5	7.3	4	56
	45.67	38.39	2016	9	26	2.5	8	20	35
	45.71	38.35	2016	9	27	3.7	5	18	18
	45.67	38.38	2016	10	7	2.6	4	7	13
	45.40	38.40	2016	12	26	2.9	18.3	1	55

	Longitude	Latitude	Year	Month	Day	Magnitude	Depth	Hour	Minute
	45.34	38.41	2017	12	4	2.5	7	7	0
	45.37	38.43	2018	1	13	3.2	6	0	50
	45.69	38.38	2018	3	4	2.6	6	8	16
	45.33	38.41	2018	3	30	2.7	4	10	10
	45.40	38.41	2018	4	30	3.4	11	5	49
	45.66	38.38	2018	6	19	2.6	9	2	56
	45.66	38.38	2018	9	4	2.6	6.4	1	50
	45.42	38.41	2018	11	21	3.3	5	0	42
	45.45	38.42	2018	12	26	3.5	5	7	41
	45.33	38.42	2019	4	11	2.7	10	9	14
	45.33	38.42	2019	4	12	3.4	6	0	16
	45.35	38.43	2019	4	12	3.8	6	4	12
	45.33	38.43	2019	4	12	2.7	6	6	14
	45.39	38.40	2019	6	8	2.8	6	0	54
	45.44	38.39	2019	6	8	2.5	6	1	0
	45.44	38.43	2019	6	9	2.8	4.9	4	14
SBF	47.47	37.67	2013	1	15	2.7	13.1	5	31
	47.42	37.71	2015	12	28	3.5	9	10	3
	47.44	37.71	2019	4	15	2.7	6.8	6	22

Triggering of the 2012 Ahar-Varzaghan earthquake doublet (Mw6.5&6.3) by the Sahand Volcano and North Tabriz fault (NW-Iran); Implications on the seismic hazard of Tabriz city

Seyyedmaalek Momeni[1,2*]
1. EPFL Geo-Energy Lab – Gaznat Chair on Geo-Energy, EPFL-ENAC-IIC-GEL, Station 18, CH-1015, Lausanne, Switzerland.
2. International Centre for Theoretical Physics (ICTP), Trieste, Italy.
***** Corresponding author, E-mail: maalek.momeni@gmail.com

Abstract

Seismic history of the North Tabriz fault (NTF), the main active fault of Northwestern Iran near Tabriz city, and its relation to the Sahand active Volcano (SND), the second high mountain of the NW Iran, and to the 11 August 2012 Ahar-Varzaghan earthquake doublet (Mw6.5&6.3) (AVD), is investigated. I infer that before AVD seismicity of the central segment of NTF close to SND was very low compared to its neighbor segments. Magmatic activities and thermal springs near central NTF close to Bostan-Abad city and low-velocity anomalies reported beneath SND toward NTF in tomography studies suggest that the existing heat due to SND magma chamber has increased the pore-fluid pressure that overcomes the effective normal stress on the central NTF, resulting in its creep behaviour. Two peaks of cumulative scalar seismic moments of earthquakes observed on both lobes of the creeping segment, confirming the strong difference in the deformation rate between these segments. On 2012, AVD struck in the 50 km North of NTF, in the same longitude range to SND and with the same right-lateral strike-slip mechanism to

NTF, as a result of partial transfer of the right-lateral deformation of NW Iran toward the North of NTF on the Ahar-Varzaghan fault system. A cumulative aseismic slip equal to an Mw6.8 event is estimated for the creeping segment of NTF, posing half of the 7mmy-1 geodetic deformation has happened in the creep mode. This event has transferred a positive Coulomb stress field of >1 bar on the AVD and triggered them. Also, the western and eastern NTF segments received >4 bar of positive Coulomb stresses from the creeping segment and are probable nucleation locations for future earthquakes on NTF. The observed creep may be the reason for the NTF segmentation during the 1721AD M7.6 and 1780 AD M7.4 historical earthquakes.

Keywords: Induced seismicity; aseismic deformation; pore-fluid pressure; effective stress; volcano; triggering

1. Introduction

On 11 August 2012, an earthquake doublet with Mw6.5 and Mw6.3 occurred in NW Iran near the Ahar and Varzaghan cities (AVD), 40 km Northeast of Tabriz city (TBZ), the fourth megacity of Iran with >2 million population. They located in 50 km North of Sahand Volcano (SND), which situated 40 km Southeast of TBZ. AVD caused >300 fatalities. In terms of mechanism, the first mainshock exhibits an almost pure right-lateral strike-slip faulting, and the second one had two slip patches with right-lateral strike-slip and reverse mechanisms (Fig. 1a, Momeni & Tatar, 2018; Momeni et al, 2019). The first mainshock produces almost 12 km of surface rupture. The mainshocks mechanisms and their rupture geometries were almost the same to the North Tabriz Fault (NTF), the main active fault of northwestern Iran, that crosses just

North of TBZ. Before AVD, the seismicity on the Ahar-Varzaghan fault system was negligible, so that these events were a surprise in that region.

1.1. <u>Tectonic Settings</u>

NW of Iran is a part of Turkish-Iranian plateau, bounded by the Caucasus Mountains to the North, Zagros Fold and thrust belt to the South, and Talesh Mountains to the East. This region is under complex tectonics which resulted in high deformation and seismic activity (Berberian and Arshadi, 1976; Jackson, 1992; Ghods et al., 2015; Momeni & Tatar, 2018) (Fig. 1). The main tectonic regime is the oblique convergence of Arabia-Eurasia with the current deformation rate of about 13–15 mmy−1, at the longitude of 46.1 °E (Vernant et al., 2004; Reilinger et al., 2006). The Talesh Mountains on the eastern termination of the region is either colliding to the relatively thick South Caspian sedimentary cover (~20 km) (Zamani and Masson, 2014) or, the South Caspian crust is under-thrusting westward beneath it (Jackson et al., 2002). Two different northeastward and northwestward deformation directions are observable in the GPS velocity vectors at the longitude of 44°E, which suggest it as the western margin of the region (Momeni & Tatar, 2018).

Earthquakes mechanisms (GCMT) and surface deformation studies (Reilinger et al., 2006; Djamour et al., 2011) suggest the resulting deformation in NW Iran is mainly the right-lateral strike-slip faulting on the W-NW striking faults within the region. While thrust faulting is partitioned to the North on the Great Caucasus (Jackson, 1992; McClusky et al., 2000; Momeni & Tatar, 2018). The two N-S to NE- SW (N018°) shortening and NW-SE (N287° and N155°) strike-slip deformation stress regimes were obtained by Zamani and Masson, (2014). The first stress system developed the three E-W striking fold and thrust belts, Arasbaran, Ghoshe-dagh and Bozkosh mountain ranges. While the N-S striking structures like Talesh mountains corresponds to the second stress system (Fig. 1a).

NTF with the main right-lateral strike-slip mechanism and deformation rate of 7 ± 1 mmy−1 accommodates most of the deformation of the region (Djamour et al., 2011). Rizza et al., (2013) estimated that the current deformation rate has been mostly constant since late quaternary until now (during the past 45 ka). However, they remarked a decrease in the strike-slip deformation rates along the NTF from about 7 mmy−1 to 5 mmy−1 from the West to the East of 47° longitude, and they relate it to the fault orientation changes from about NW-SE to W-E (Djamour et al., 2011; Rizza et al., 2013) (Fig. 2a). Later, Su et al., (2017) reported subsidence in the closest GPS station to the Northeast SND near BA and interpreted it as magmatic activities of Sahand.

A microseismicity study along the NTF using a local seismic network confirmed the main shear deformation mechanism of NTF in the upper crust (Moradi et al. 2011). On the western and eastern terminations of NTF, the North Mishu Fault (NMF) and the South Bozkosh Fault (SBF) are the two oblique reverse faults with right-lateral strike-slip components that strike ~E-W and dip to the South and North, respectively. Solaymani Azad et al., (2015) called the NTF, NMF, and SBF as Tabriz Fault System (TFS).

Before the occurrence of the 2012 earthquake doublet, the Ahar-Varzaghan fault system has been in a long seismic quiescence (Momeni & Tatar, 2018; Fig. 1a). However, field observations revealed the continuation of fault to the both East and West of the ruptured segment during the

2012 AVD (e.g. Copley et al. 2013, Donner et al. 2015, Ghods et al. 2015). The clear segmentation has been observed along this fault system with different kinematics and without clear connections that suggest it as a young fault system (Donner et al., 2015). The occurrence of the AVD suggested that some of the shear strain of the region is not compensating by the NTF, specifically at the longitudes east of 46°E (Donner et al. 2015; Ghods et al. 2015).

Sahand volcano with 3707 m elevation is an isolated, extensively distributed (~3000 km2 area) stratovolcanic complex (Ghalamghash et al., 2019). Together with Sabalan and Saray, they are three Late Miocene-Quaternary volcanoes that formed as results of the collision between the Arabian and Eurasian plates along the Neo-Tethyan suture zone in NW Iran. The formation of Neo-Sahand is estimated to ca. 600 to b173 ka (Ghalamghash et al., 2019). They mostly observed within and outside of the widely eroded caldera margin. Neo-Sahand units include basaltic andesitic to rhyolitic domes in the center of the complex as well as small parasitic cones along with subvolcanic dikes toward the northeast.

1.2. Historical earthquakes of NW Iran

Historical seismicity is widely distributed in the region, and mostly on the NTF and NMF. Tabriz city has been the capital of Iran and Azerbaijan in the past. Several large destructive historical earthquakes (magnitudes up to Ms=7.6) have reported for Tabriz (Ambraseys and Melville, 1982; Berberian and Yeats, 1999). Most of them are related to the activity of NTF (Fig. 1a). The last two M>7 destructive historical earthquakes have occurred on 1721 AD and 1780 AD, that ruptured more than 50 km of the southeastern and northwestern segments of the NTF and caused over 40,000 and 200,000 fatalities, respectively (Ambraseys and Melville, 1982; Berberian and Yeats, 1999; Momeni & Tatar, 2018).

Paleoseismological studies revealed at least three major (M~7.5) historical earthquakes for the southeastern segment over the past 33.5 ka, including the 1721 AD M7.6–7.7 earthquake (Solaymani Azad et al., 2015). On the other side, four historical earthquakes are reported for the northwestern segment of the NTF during the past 3.6 ka, the most recent being the Ms~7.4 1780 AD earthquake (Hessami Azar et al., 2003). The estimated slip per event and slip rate on this segment are 4 ± 0.5 m and 3.1–6.4 mmy−1, respectively, and the average recurrence interval of large earthquakes on it is estimated in the range of 350 to 1430 years.

NMF and SBF also ruptured during historical earthquakes, the last two being the 1786 AD Marand and 1593 AD Sarab earthquakes that suggest a seismic migration from the southeast toward the northwest of TFS. They also reveal earthquake clustering (e.g. Kagan and Jackson, 1991; Berberian, 1997; Karakhanian et al., 2004) and interaction between fault segments of the TFS (Solaymani Azad et al., 2015).

1.3. Instrumental earthquakes of NW Iran

Mechanism of deformation strongly changes from the western Alborz to the Iran-Turkey borders. The 1976 Mw7.0 Chalderan earthquake has occurred near the borders of Iran with Turkey on the right-lateral strike-slip Chalderan-Khoy fault that strikes E-W. While, the 1990 Mw7.4 Rudbar-Tarom earthquake on the western Alborz mountains has occurred on a left-lateral strike-slip fault trending WNW- ESE (Momeni & Tatar, 2018).

Within the NW Iran before the AVD, the 1997 Mw = 6.1 Ardebil earthquake occurred on an N-S striking fault situated ~150 km East of the AVD, showing a pure left-lateral strike-slip faulting (Aziz Zanjani et al., 2013). On 11 August 2012, the AVD occurred that were very well recorded by different instruments. The first mainshock with Mw6.5 had a right-lateral strike-slip mechanism. While the second one with Mw6.3 was more complex and contained two slip patches: the first patch had a right-lateral strike-slip mechanism, and the second one had a reverse mechanism (Momeni et al., 2019). The last large earthquake in the region is the 7 November 2019 Mw5.9 Torkamanchay earthquake (TKC) that occurred on an NE striking left-lateral strike-slip fault between North and South Bozkosh Faults (Valerio et al., 2020).

The EHB catalog (Engdahl et al., 2006) shows most of the seismicity on the Talesh mountains and also on the NMF (Fig. 1a). However, no large earthquake (M>5) reported on the segments of NTF in the GCMT catalog (Fig. 1b).

In 1995 a local permanent seismic network consisting of eight stations, known as Tabriz sub-network of the Iranian Seismological Center (IRSC), was installed in the region (Fig. 1b). However, this sparse network (station spacing ~50 km) limited the number of precisely located earthquakes. There are only 70 earthquakes in IRSC catalog from 1995 until the end of 2005, and none of them has located close (distance <5km) to NTF. From 2006, after the installation of the Broadband Iranian Network (BIN) maintained by the International Institute of Earthquake Engineering and Seismology (IIEES) in Tehran, Iran, and improvement of IRSC network data, the IRSC locations improved in terms of accuracy and magnitude completeness.

Figure 1b shows the precisely located seismicity of the region recorded in the IRSC network from 1995 until the occurrence of AVD in August 2012. They have located by at least five stations, have a location error of <5 km, RMS of <0.5 s, and azimuthal gap of <270°. They are all smaller than Mw5.0 unless the 1997 Ardabil earthquake. They mostly have shallow focal depths (< 20 km) and are distributed mainly along the NTF and NMF. However, the central segment of NTF near SND shows much lower seismic activity compared to the western and eastern segments (Fig. 1b). A seismic cluster on the North of AVD is mainly related to mining activities in that area. The rest of the seismicity is related to the Astaneh (ASF), West Alborz (WAF), South Qoshadagh (SQF), Goshachay (GCF), South Bozkosh (SBF), North Mishu (NMF), Maragheh (MGF), Khajeh (KHF), and Nehram (NHF) faults. After AVD, the only large event of the region is the 7 November 2019 Mw5.9 Torkamanchay earthquake that occurred on an NE striking vertical dip fault between NBF and SBF near the eastern termination of NTF.

Detailed microseismic monitoring on the NTF by a local dense seismic network data confirmed its right-lateral strike-slip mechanism with an East-Southeastward oriented fault plane (Moradi et al., 2011; Fig. 4). Microearthquakes located by Moradi et al., (2011) on NTF situated in the upper crystalline crust at depths shallower than 20 km. Moradi et al. proposed a vertical dip fault plane for the NTF.

1.4. <u>The goal</u>

In this study, the seismic activity of the NTF from historical earthquakes until 2020 is investigated. A cumulative slip model has proposed for the creeping segment of NTF near SND, and, the transferred Coulomb stress by this aseismic deformation on the AVD ruptures has computed. Ultimately, the relation between NTF seismic-aseismic deformation activity to SND and AVD, and changes in the rheology of the central segment of NTF near SND after AVD investigated.

2. Seismicity along NTF and NMF

As mentioned before, earthquake locations by IRSC seismic network in NW Iran started in 1995. However, the IRSC catalog is poor until the end of 2005 due to data quality and sparsely distanced stations (>50 km). There are no earthquakes in the distance of 5 km to the NTF from 1995 to the end of 2005. From 2006, earthquake monitoring has improved in this region in terms of location accuracy and magnitude completeness.

The well-located earthquakes in the distance of 5 km to NTF and NMF are selected from 2006 until before the AVD and from AVD until November 2019 TKC in the IRSC network. These sets are recorded in >=5 stations, with location errors of <5 km, RMS of <0.5 s, and azimuthal gap of < 270°. The first set contains 512 earthquakes in which 45 of them have magnitudes 2.5 and higher. I infer that the central segment of NTF near SND has a long quiescence from 2006 until the occurrence of AVD. However, the two nearby segments show high seismicity (Fig. 2a).

After AVD, 69 M>=2.5 earthquakes are in 5 km distance to NTF and NMF (IRSC catalog) with a distributed seismicity and their most concentration on the NMF (Fig. 2b; Table S3). However, the two relatively large events (3.7<M<4.0) are located in the central NTF near SND (Fig. 2b).

The cumulative scalar seismic moments of the earthquakes that occurred after 2006 until the 2012 AVD, and after that until TKC, is computed to investigate the seismic energy release behaviour along the NTF and NMF. The cumulative scalar seismic moment plot of the first set shows two peaks in the Eastern and Western lobes of central NTF that matches to SND, and one on the NMF (Fig. 2b). However, the central NTF itself was almost silent.

For earthquakes that occurred on NTF After AVD, the cumulative scalar seismic moment plot shows a peak in the middle of the central NTF. However, the previously observed peaks of the scalar seismic moment on its lobes are disappeared (Fig. 2b). There is also a relatively wide peak on the NMF, North of Urmieh Lake, where the high seismicity was also observed before AVD.

3. <u>Creeping segment of NTF near SND</u>

Creeping behaviour is mainly related to frictional strength of the fault zone material, depending on lithology, temperature, and pore-fluid pressure (i.e. Avouac, 2015, Khoshmanesh & Shirzaei, 2018). The magmatic activities reported in a GPS study by Su et al., (2017) near BA, known thermal springs there, and absence of seismic activity from 2006 until 2012 AVD on the central NTF near BA, propose that the existing heat due to the SND magma chamber decrease the effective normal stress on this segment of the fault by increasing the pore-fluid pressure on the fractured fault area and consequently cause it to creep. The resulting different deformation rates along NTF segments is probably the reason for the observed two peaks of high cumulative scalar seismic moments on both lobes of central segment of NTF near SND.

To prove this idea, a cumulative aseismic deformation on the central segment of NTF is estimated. This segment didn’t rupture since the 1721 M7.6 historical earthquake and the GPS study by Djamour et al., (2011) and Rizza et al., (2013) suggest right-lateral deformation of 7mmy-1 for this segment. A maximum slip of 0.007*(2012-1721) =2.04 meters is expected for this segment until the AVD. This segment has a strike/dip of 300°/90° and covers the silent central segment of NTF with a length of ~30 km and locking depth of ~20 km that is suggested by Djamour et al., (2011). I stress that Rizza et al., (2013) suggested a relatively unchanged deformation rate on NTF since 65 ka. If I fairly pose that only half of this deformation has happened in creep mode and the other half is locked (and may rupture in a future earthquake), the slip model will have a maximum value equal to 1.02 m. Later in section 4, I will explain that even considering the smaller contribution of creep in the whole deformation (i.e. 25%), the transferred stress field by the creeping segment will be high enough to trigger the AVD. An elliptical slip patch (i.e. Ruiz & Madariaga, 2013; Momeni et al., 2019) is proposed with a max slip of 1.02 m at the center and with a Gaussian distribution of slip and half of the max slip equal to ~51 cm on the borders, where high seismic activity is observed (Fig. 2a). The resulting source has a scalar seismic moment of ~2.0*e+19 Nm equal to an Mw6.8 earthquake. For a fully creeping slip model, the source will have a scalar seismic moment of ~4.0*e+19 Nm equal to an Mw7.0 earthquake.

The resulting deformation may transfer positive Coulomb failure stresses on the nearby faults. I note that AVD has occurred in the same longitude to this creeping segment, suggesting that the right-lateral deformation does not fully release on NTF and probably some of it transfer toward North, as also suggested by Donner et al., (2015) by geological investigations.

4. Stress transfer

4.1. Stress transfer from the creeping segment of NTF to AVD

The stress tensor produced by the defined slip model for the creeping segment of NTF is calculated on a 3-D grid in the region using a method by Wang et al. (2003) (Fig. 3). The method is based on the dislocation theory that is implemented in a multilayered media. A 1-D crustal velocity model of the area retrieved from precisely located aftershocks of AVD is used, and a

Poisson ratio of ~0.25 obtained from a Vp/Vs ratio of 1.74 (Momeni & Tatar 2018, Table S1). The Coulomb stress field is calculated on optimally oriented ruptures of both Ahar-Varzaghan earthquakes, and by considering strike-slip mechanisms of their slip patches obtained by Momeni et al., (2019).

A positive Coulomb stress of >1 bar is transferred from the creeping segment on the ruptured areas during the doublet (Fig. 3a). Also, the creeping segment had positive coulomb stress transfer of >4 bar on the nearby segments and excited them to slip (Fig. 3b), especially on the western segment of NTF (e.g., Vadacca, 2020).

4.2. Stress transfer from AVD to NTF

The stress tensor produced by the AVD ruptures that were obtained in a study by Momeni et al., (2019) is computed on the region using the same method mentioned in section 4.1. As was also reported by Momeni et al., (2019), the stress field shows a positive Coulomb stress transfer of >0.1 bar on most of the creeping segment of NTF, and also ~0.1 bar on the NBF (Fig. 4a). The two peaks of cumulative scalar seismic moments of earthquakes are observed in these segments on NTF and NBF from the 2012 AVD until the 2019 TKC (Fig. 2b).

A cumulative positive normal stress transfer of >0.1 bar is obtained from AVD on most of the creeping segment of NTF (Fig. 4b). This additional positive normal stress to the regional stress may increase the effective normal stress on the creeping segment and change its rheology from partial creep to more stick-slip. The occurrence of two earthquakes on the proposed creep segment after the AVD which is also observed as a peak of the scalar seismic moment in Figure 2d confirms our suggestion.

On the NMF, two a wide peak of the cumulative scalar seismic moment was observed North of Urmieh Lake before AVD. While after the doublet, there is a peak of the cumulative scalar seismic moment in between of the previous wide peak suggesting that this part was partially locked, and has been excited by the doublet. Also, these seismic activities may be partly related to the relatively higher pore-fluid pressure provided by the Urmieh Lake on the NMF, or by the recent dramatic decrease of 90% of the water volume of the lake during years 1995 to 2013 (Schulz et al., 2020) that may reduce the effective normal stress on NMF, unclamp it, and excite it to slip.

5. Discussion

The seismicity of the NTF and NMF is investigated from documented historical earthquakes to November 2019 TKC earthquake. Many historical earthquakes are referred to NTF (Fig. 1a). The last two historical earthquakes of 1721 AD and 1780 AD cover all NTF segments. EHB catalog shows most of the seismic activity on the western termination of NTF. However, the GCMT catalog does not have any earthquake on the NTF.

The IRSC network earthquake catalog has improved from 2006 in terms of completeness and location accuracy. There are 512 earthquakes (45 of which have Ml>=2.5; Table S2) in the distance of 5 km from NTF and NMF for a period from 2006 until before AVD. These seismic activities are distributed along all segments of NTF and NMF unless the central segment of NTF that is situated North of SND and shows much less seismicity compared to its neighbor segments. Two remarkable peaks are observable in the cumulative scalar seismic moments of these earthquakes on both lobes of the central segment of NTF near SND (Figure 2b). A probable explanation for such behaviour is that the segment of NTF near SND is partially creeping. Djamour et al., (2011) and Rizza et al., (2013) reported a decrease in right-lateral surface deformation rate from West of BA (Longitude 47°) to the East from 7mmy-1 to 5mmy-1. Su et al., (2017) remarked that the region near BA is affected by deep magmatic activities of SND. This segment is close to the thermal areas (hot springs) near BA reported by Ghalamghash et al. (2019). Tomography studies by Rezaeifar et al., (2016) and Bavali et al., (2016) revealed a heterogeneous structure in this region with high and low-velocity anomalies. A low-velocity region has obtained beneath SND at depths deeper than 8 km that extends until the NTF by Bavali et al., (2016) (Fig. 5). However, at shallower depths, a relatively high-velocity anomaly obtained by Rezaeifar et al., (2016), and interpreted as cooled magmatic rocks of SND. The observed thermal activities near BA area are probably due to the existence of some dyke-like branches of the SND deep magma chamber in that area that was also suggested by Ghalamghash et al. (2019) as many young craters with dacitic to rhyolitic parasitic cones of magma of neo-Sahand were observed toward NNE of SND near BA (see Fig. 3). The other explanation will be the possible aid of NTF fractured area which is extended down to the depth of 20 km, in bringing heat to the surface. The existing heat increases the pore-fluid pressure in the fault area and unclamps this segment of NTF, facilitating its creep.

However, this segment of NTF was ruptured as a part of the 1721 AD M7.6 earthquake. Harris, (2017) mentioned that the creeping segments are also potential to rupture in M~6.8 earthquakes, and they usually rupture together with their nearby segments (i.e. Van den Ende et al., 2020). Dynamic weakening is the probable mechanism for rupture of such fault segments (i.e. Noda & Lapusta, 2013). The same mechanism may have happened during the 1721 AD earthquake, and that is most likely the reason for segmentation of NTF during 1721 AD and 1780 AD historical earthquakes.

The effect of raise of pore-fluid pressure in facilitating the fault creep/slip is widely observed and reported mostly for Strike-slip faulting mechanism (e.g. Avouac, 2015, Floyd et al., 2016, Goebel et al., 2017, Scuderi et al., 2017, Michel et al., 2018, Johann et al., 2018, Eaton & Schultz, 2018, Zhu et al., 2020, Momeni & Madariaga, 2020).

A slip model is estimated for the creeping segment of NTF from 1721 AD until before the 2012 AVD considering that half of the 7 mmy-1 right-lateral deformation rate obtained by Djamour et al., (2011) and Rizza et al., (2013) was happening in creep mode. This creep has occurred at the longitudes between 46.55° E to 46.85° E and with a locking depth of 20 km. Having a maximum cumulative slip of 1.02m, the obtained cumulative scalar seismic moment is 2.0 * e+19 Nm equal to Mw6.8 (for the fully creep mode, this value raises to 4.0 * e+19 Nm equal to Mw7.0). This also remarks that the other segments of NTF have a considerable amount of accumulated tectonic stress.

The creeping segment of NTF transferred positive Coulomb stress field of >4 bar on the neighbor segments, and brought them closer to failure (Fig. 3b). That is confirmed by the observation of two peaks of cumulative scalar seismic moments on both lobes of the creeping segment. These earthquakes can be considered as aftershocks of the creep event. Aftershocks surrounding a slip model is a consistent feature of large earthquakes (see Henry & Das, 2002).

The 3D stress field produced by this creep source on AVD is computed. The estimated slip model for the creeping segment can transfer positive Coulomb stress of >1 bar on the AVD and trigger them (Fig. 6). After the AVD until November 2019, one peak of the cumulative scalar seismic moment is observed for earthquakes occurred in 5 km distance from NTF, and that is in the middle of the central NTF. There is also one peak on the NMF. Observation of seismic activity on the previously creeping segment of NTF and absence of two peaks of cumulative scalar seismic moments on both lobes of that segment suggest a change in its rheology from creep to stick-slip after AVD. This change is probably due to the positive static normal stress field of >0.1 bar that was transferred from AVD on half of the creeping segment of NTF. Also, Momeni et al., (2019) compute the stress field by AVD on NTF and NMF and reported transfer of positive Coulomb stress of >0.1 bar on the central segment of NTF as well as NMF. For the NMF, two relatively small peaks of cumulative scalar seismic moment release are observed before the AVD (Fig. 2b). After AVD, one big peak is observed in between the two previous peaks suggesting that this part of NMF was partially locked, and triggered by the 2012 AVD.

Seismic quiescence of the creeping segment of NTF near SND from 2006 together with the observed magmatic activities in that area proposes a strong relation between the volcanic activity of SND and frictional properties of that segment of NTF. Compared to the central NTF, the western segment that is closer to the Tabriz city shows higher seismic activity. Also, the Eastern segment shows considerable seismic activity which highlights its importance as another potential segment of the NTF for future large earthquakes.

The smooth geometry of the central and western segments of NTF may facilitate the rupture expansion on them. However, low seismic coupling in the creeping central NTF may act as a barrier and stop ruptures from expansion toward the western segment.

The suggested 20km thick seismogenic layer for NTF (Djamour et al., 2011; Moradi et al. 2011), highlights its potential for the production of large earthquakes and with low-frequency seismic energy contents that can reach to Tabriz city with less damped energy and affect the tall buildings.

6. Conclusion

I infer a seismic quiescence in the central segment of the NTF, North of SND from 2006 until August 2012 AVD. While the two eastern and western segments of NTF show much higher seismicity with two remarkable peaks of cumulative scalar seismic moments on both lobes of the central segment near SND. The existing heat by the SND magma chamber near the fractured area of central NTF raises the pore-fluid pressure and decreases the effective normal stress there, consequently unclamp the fault, and facilitate the right-lateral creep. An Mw6.8 half-creep slip model is suggested for this segment considering half of 7 mmy-1 constant geodetic deformation rate on it since the 1721 AD historical earthquake.

The creeping segment is situated in almost the same longitude range to the 2012 AVD and transferred positive Coulomb stress fields of >1 bar on them. This segment also transferred >4 bar of positive Coulomb stress on its neighbor segments, where the two peaks of cumulative seismic moments were observed. Some of the right-lateral deformation stresses on central NTF transferred to the North and released during the 2012 AVD on the Ahar-Varzaghan complex fault system (Fig. 6).

After the AVD until TKC, two new peaks of the cumulative scalar seismic moment have observed for earthquakes that occurred on NTF and NMF. One is exactly in the middle of the previously creeping central segment of NTF, consistent to the obtained transfer of positive normal and Coulomb stresses on this segment by AVD (i.e. Momeni et al., 2019). The transferred stress changed the rheology of the creeping segment from mostly creeping to temporary stick-slip.

The other peak of the cumulative scalar seismic moment is on the NMF North of Urmieh Lake, and, may be due to the existing pore-fluid pressure or a recent dramatic decline in the water level of the lake over the past two decades (90% decrease in its volume has happened during 1995 to 2013; Schulz et al., 2020) that both reduce the effective normal stress on NMF, unclamp it, and facilitate slip on it (e.g. Saar & Manga, 2003).The two peaks of cumulative scalar seismic moments observed before AVD on the western and eastern lobes of the creep segment of NTF near SND were disappeared after AVD until November 2019 TKC, suggesting a change in seismic activity of NTF along its segments by the transferred stress fields produced by AVD, at least for the first 8 years. This change is probably temporary and NTF will return to continue its creep behaviour in the central segment near SND.

In terms of rupture dynamics, the two highly stressed neighbor segments of NTF are prone to nucleate earthquakes (e.g. Vadacca et al., 2020). If an earthquake nucleates on the stressed lobes of the creeping segment and its rupture grow toward the West, it will cause a strong directivity effect for that earthquake toward Tabriz city. However, the creeping segment may work as a barrier and probably does not allow NTF to rupture in both Central and Western segments in one larger earthquake.

The change in seismic activity on the different segments of NTF and having mix behaviour of lock and creep deformation on them raise the seismic hazard in the region, especially for the Tabriz city that currently host > 2 million people. I suggest continuous monitoring of seismicity along NTF will help to understand the rheological behaviours of segments of this mature fault system, with a concentration on the central and western segments that did not rupture in large events since the 1721 AD and 1780 AD historical earthquakes.

7. Data and Resources

The earthquakes data are available through the Iranian Seismological Center (IRSC) network website (http://irsc.ut.ac.ir). The earthquake focal mechanisms in Figure 1b are from the GCMT catalog (http://www.globalcmt.org/CMTsearch.html last access on August, 2020). The supplementary data includes velocity model of the area and earthquakes hypocenters information.

8. Acknowledgements

This research did not receive any specific grant from funding agencies in the public, commercial, or not-for-profit sectors. I thank IRSC and IIEES networks for providing the seismic data. Figures plotted using Generic Mapping Tools (GMT) (http://gmt.soest.hawaii.edu/), Paraview software (https://www.paraview.org), and personal codes in Matlab environment (https://www.mathworks.com).

9. References

Ambraseys, N.N. & Melville, C.P., 1982. A History of Persian Earthquakes, Cambridge Univ. Press. https://doi.org/10.1016/j.jseaes.2008.08.001

Avouac, J.P., 2015. From Geodetic Imaging of Seismic and Aseismic Fault Slip to Dynamic Modeling of the Seismic Cycle, Annu. Rev. Earth Planet. Sci. 2015. 43:233–71, doi: 10.1146/annurev-earth-060614-105302.

Aziz Zanjani, A., Ghods, A., Sobouti, F., Bergman, E., Mortezanejad, G., Priestley, K., Madanipour, S., Rezaeian, M., 2013. Seismicity in the western coast of the South Caspian Basin and the Talesh Mountains. Geophys. J. Int. 194, 799–814. https://doi.org/10.1093/gji/ggt299

Bavali, K., Motaghi, K., Sobouti, F., Ghods, A., Abbasi, M., Priestley, K., Mortezanejad, G., Rezaeian, M., 2016. Lithospheric structure beneath NW Iran using regional and teleseismic travel-time tomography, Physics of the Earth and Planetary Interiors 253, 97–107. http://dx.doi.org/10.1016/j.pepi.2016.02.006

Berberian, M., Arshadi, S., 1976. On the evidence of the youngest activity of the North Tabriz Fault and the seismicity of Tabriz city. Geol. Surv. Iran Rep. 39, 397–418.

Berberian, M., 1997, Seismic sources of the Transcaucasian historical earthquakes. In S. Giardini and Balassanian, S. (Eds.), Historical and prehistorical earthquakes in the Caucasus. Kluwer Academic Publishing, Dordrecht, Netherlands, pp. 233–311.

Berberian, M. & Yeats, R.S., 1999. Patterns of historical earthquake rupture in the Iranian Plateau. Bulletin of the Seismological Society of America **89**, 120–139.

Berberian, M. & Yeats, R.S., 2001. Contribution of archaeological data to studies of earthquake history in the Iranian Plateau. Journal of Structural Geology **23**, 563–584.

Copley, A., Faridi, M., Ghorashi, M., Hollingsworth, J., Jackson, J., Nazari, H., Oveisi, B., Talebian, M., 2013. The 2012 August 11 Ahar earthquakes: consequences for tectonics and earthquake hazard in the Turkish-Iranian plateau. Geophys. J. Int. 196, 15–21. http://dx.doi.org/10.1093/gji/ggt379

Djamour, Y., Vernant, P., Nankali, H.R. & Tavakoli, F., 2011. NW Iran eastern Turkey present-dat kinematics: results from the Iranian permanent GPS network, Earth planet. Sci. Lett., 307, 27–34. http://dx.doi.org/10.1016/j.epsl.2011.04.029

Donner, S., Ghods, A., Krauger, F., Roßler, D., Landgraf, A. & Ballato, P., 2015. The Ahar-Varzeghan earthquake doublet (Mw 6.4 and 6.2) of 11 August 2012: regional seismic moment tensors and a seismotectonic interpretation, Bull. seism. Soc. Am., 105, doi:10.1785/0120140042.

Eaton, D.W., & Schultz, R., 2018. Increased likelihood of induced seismicity in highly overpressured shale formations, Geophysical Journal International, 214(1), 751–757, https://doi.org/10.1093/gji/ggy167.

Engdahl, E.R.; Jackson, J.A.; Myers, S.C.; Bergman, E.A.; Priestley, K. Relocation and assessment of seismicity in the Iran region. Geophys. J. Int. 2006, 167, 761–778. http://dx.doi.org/10.1111/j.1365-246X.2006.03127.x

Floyd, M.A., et al., 2016. Spatial variations in fault friction related to lithology from rupture and afterslip of the 2014 South Napa, California, earthquake, Geophys. Res. Lett., 43, doi:10.1002/2016GL069428.

Ghalamghash, J., Schmitt, A.K., Chaharlang, R., 2019. Age and compositional evolution of Sahand volcano in the context of post-collisional magmatism in northwestern Iran: Evidence for time-transgressive magmatism away from the collisional suture, Lithos 344–345 (2019) 265–279, https://doi.org/10.1016/j.lithos.2019.06.031.

Ghods, A., Shabanian, E., Bergman, E., Faridi, F., Donner, S., Mortezanejad, G., Aziz-Zanjani, A., 2015. The Varzaghan-Ahar, Iran, Earthquake Doublet 1 (Mw 6.4, 6.2): implications for the geodynamics of northwest Iran. Geophys. J. Int. 203, 522–540. http://dx.doi.org/10.1093/gji/ggv306

Goebel, T.H.W., Weingarten, M., Chen, X., Haffener, J., Brodesky, E.E., 2017. The 2016 Mw5.1 Fairview, Oklahoma earthquakes: Evidence for long-range poroelastic triggering at >40 km from fluid disposal wells, Earth and Planetary Science Letters, 472, 50-61. https://doi.org/10.1016/j.epsl.2017.05.011

Harris, R. A. (2017), Large earthquakes and creeping faults, Rev. Geophys., 55, 169-198, doi:10.1002/2016RG000539.

Henry, C., & S. Das, 2002. The Mw 8.2 17 February 1996 Biak, Indonesia, earthquake: Rupture history, aftershocks, and fault plane properties, J. Geophys. Res., **107**(B11), 2312, doi: 10.1029/2001JB796.

Hessami Azar, K., Pantosti, D., Tabassi, H., Shabanian, E., Abbasi, M.R., Feghhi, K., Solaymani, S., 2003. Paleoearthquakes and slip rates of the North Tabriz Fault, NW Iran: preliminary results. Ann. Geophys. 46, 903–915. DOI: https://doi.org/10.4401/ag-3461

Jackson, J., 1992. Partitioning of strike-slip and convergent motion between Eurasia and Arabia in Eastern Turkey and the Caucasus. J. Geophys. Res. 97, 12471–12479. https://doi.org/10.1029/92JB00944

Jackson, J., Priestley, K., Berberian, M., 2002. Active tectonics of the South Caspian Basin. Geophys. J. Int. 148, 214–245. https://doi.org/10.1046/j.1365-246X.2002.01588.x

Johann, L., Shapiro, S.A. & Dinske, C., 2018. The surge of earthquakes in Central Oklahoma has features of reservoir-induced seismicity. Sci Rep 8, 11505. https://doi.org/10.1038/s41598-018-29883-9.

Kagan, Y. Y., and Jackson, D. D., 1991, Long-term earthquake clustering, Geophys. J. Int., 104, 117–133. https://doi.org/10.1111/j.1365-246X.1991.tb02498.x

Karakhanian, A., Jrbashyan, R., Trifonov, V., Philip, H., Avagyan, A., Hessami, K., Jamali, Bayraktutan, F. M., Bagdassarian, H., Arakelian, S., Davtyan V., and Adilkhanyan, A., 2004, Active faulting and natural hazards in Armenia, eastern Turkey and Northern Iran, Tectonophysics, 380, 189–219. https://doi.org/10.1016/j.tecto.2003.09.020

Khoshmanesh, M., Shirzaei, M., 2018. Episodic creep events on the San Andreas Fault caused by pore pressure variations, Nat. Geosci. https://doi.org/10.1038/s41561-018-0160-2

Masson, F., Djamour, Y., Van Gorp, S., Chery, J., Tatar, M., Tavakoli, F., Nankali, H. & Vernant, P., 2006. Extension in NW Iran driven by the motion of the South Caspian Basin, Earth planet. Sci. Lett., 252, 180–188. https://doi.org/10.1016/j.epsl.2006.09.038

Michel, S., Avouac, J.P., Jolivet, R., and Wang, L., 2018. Seismic and Aseismic Moment Budget and Implication for the Seismic Potential of the Parkfield Segment of the San Andreas Fault, Bulletin of the Seismological Society of America, Vol. 108, No. 1, pp. 19–38, Doi: 10.1785/0120160290.

McClusky, S., et al., 2000. Global positioning system constraints on plate kinematics and dynamics in the eastern Mediterranean and Caucasus. J. Geophys. Res. 105, 5695–5719. https://doi.org/10.1029/1999JB900351

Momeni, S.M., Tatar, M., 2018. Mainshocks/aftershocks study of the August 2012 earthquake doublet on Ahar-Varzaghan complex fault system (NW Iran). Physics of the Earth and Planetary

Interiors, **283**, 67-81. https://doi.org/10.1016/j.pepi.2018.08.001

Momeni, S.M., Aoudia, A., Tatar, M., Twardzik, C. & Madariaga, R., 2019. Kinematics of the 2012 Ahar–Varzaghan complex earthquake doublet (M_w6.5 and M_w6.3), *Geophysical Journal International*, **217**, 2097–2124, https://doi.org/10.1093/gji/ggz100

Momeni, S.M., Madariaga, R., 2020. Long-term induced seismicity on the Mosha fault by Damavand Volcano, N-Iran, Implications on the seismic hazard of Tehran metropolis, under review in SRL.

Moradi, A.S., Hatzfeld, D. & Tatar, M., 2011. Microseismicity and seismotectonics of the North Tabriz Fault (Iran), Tectonophysics, 506, 22–30. https://doi.org/10.1016/j.tecto.2011.04.008

Noda, H., & Lapusta, N., 2013, Stable creeping fault segments can become destructive as a result of dynamic weakening, NATURE, **493**, 518-521, doi:10.1038/nature11703

Schulz, S., Darehshouri, S., Hassanzadeh, E. et al. 2020. Climate change or irrigated agriculture – what drives the water level decline of Lake Urmia. Sci Rep 10, 236. https://doi.org/10.1038/s41598-019-57150-y.

Su, Z., Wang, E., Hu, J., Talebian, M. & Karimzadeh, S., (2017). Quantifying the Termination Mechanism Along the North Tabriz-North Mishu Fault Zone of Northwestern Iran via Small Baseline PS-InSAR and GPS Decomposition. IEEE Journal of Selected Topics in Applied Earth Observations and Remote Sensing, vol. 10, no. 1, pp. 130-144, doi: 10.1109/JSTARS.2016.2586742.

Reilinger, R., et al., 2006. GPS constraints on continental deformation in the Africa- Arabia-Eurasia continental collision zone and implications for the dynamics of plate interactions. J. Geophys. Res. 111, B05411. https://doi.org/10.1029/2005JB004051.

Rezaeifar, M., Kissling, E., Shomali, Z.H. & Shahpasand-Zadeh, M., 2016. 3D crustal structure of the northwest Alborz region (Iran) from local earthquake tomography. Swiss J. Geosci., 1–12, Springer International Publishing. doi:10.1007/s00015-016-0219-2

Rizza, M., Vernant, P., Ritz, J., Peyrat, M., Nankali, H., Nazari, H., Djamour, Y., Salamati, R., Tavakoli, F., Chéry, J., Mahan, S., Masson, F., 2013. Morphotectonic and geodetic evidence for a constant slip-rate over the last 45 kyr along the Tabriz fault (Iran). Geophys. J. Int. 193, 1083–1094. https://doi.org/10.1093/gji/ggt041

Ruiz, S., & Madariaga, R., 2013. Kinematic and dynamic inversion of the 2008 northern Iwate earthquake, Bull. Seismol. Soc. Am., **103**(2A), 694–708, Doi: 10.1785/0120120056.

Saar, M.O., Manga, M., 2003. Seismicity induced by seasonal groundwater recharge at Mt. Hood, Oregon, Earth and Planetary Science Letters, 214, 605-618. https://doi.org/10.1016/S0012-821X(03)00418-7

Scuderi, M.M., Collettini, C., Marone, C., 2017. Frictional stability and earthquake triggering during fluid pressure stimulation of an experimental fault, Earth and Planetary Science Letters, **477**, 84-96. https://doi.org/10.1016/j.epsl.2017.08.009

Solaymani Azad, S., Philip, H., Dominguez, S., Hessami Azar, K., Shahpasandzadeh, M., Foroutan, M., Tabassi, H., Lamothe, M., 2015. Paleoseismological and morphological evidence of slip rate variations along the North Tabriz fault (NW Iran). Tectonophysics, 640–641, 20-38. https://doi.org/10.1016/j.tecto.2014.11.010

Van den Ende, M.P.A., Chen, J., Ampuero J.P. & Niemeijer A.R., 2020. Rheological Transitions Facilitate Fault‐Spanning Ruptures on Seismically Active and Creeping Faults, Journal of Geophysical Research: Solid Earth Volume 125, Issue 8, https://doi.org/10.1029/2019JB019328

Vadacca, L., 2020, The Altotiberina Low-Angle Normal Fault (Italy) Can Fail in Moderate-Magnitude Earthquakes as a Result of Stress Transfer from Stable Creeping Fault Area, Geosciences, 10, 144; doi:10.3390/geosciences10040144.

Valerio, E., Manzo, M., Casu, F., Convertito, V., De Luca, C., Manunta, M., Monterroso, F., Lanari, R. & De Novellis, V., 2020. Seismogenic Source Model of the 2019, Mw 5.9, East-Azerbaijan Earthquake (NW Iran) through the Inversion of Sentinel-1 DInSAR Measurements, Remote Sens., 12, 1346; doi:10.3390/rs12081346.

Vernant, Ph., et al., 2004. Contemporary crustal deformation and plate kinematics in Middle East constrained by GPS measurements in Iran and northern Oman. Geophys. J. Int. 157, 381–398.

Wang, R., Martin, F.L., Roth, F., (2003). Computation of deformation induced by earthquakes in a multi-layered elastic crust—FORTRAN programs EDGRN/EDCM, Computers & Geosciences 29, 195–207, 2003.

Zamani, B., Masson, F., 2014. Recent tectonics of East (Iranian) Azerbaijan from stress state reconstructions. Tectonophysics 611, 61–82.

Zhu, W., Allison, K.L., Dunham, E.M., Yang, Y., 2020. Fault Valving and Pore Pressure Evolution in Simulations of Earthquake Sequences and Aseismic Slip, Computational Physics, https://arxiv.org/abs/2001.03852.

Mailing address:

Seyyedmaalek Momeni

EPFL Geo-Energy Lab – Gaznat Chair on Geo-Energy, EPFL-ENAC-IIC-GEL, Station 18, CH-1015, Lausanne, Switzerland.

Figure Captions:

Figure 1. (**a**) Seismotectonics of the study region. Stars show the 2012 AVD hypocenter locations, and the related focal mechanisms are by Momeni & Tatar, (2018). Faults are in lines. Vectors are geodetic surface deformation rates by Masson et al., (2006), fixing the central Iran block. Hexagons are historical earthquakes (Ambraseys & Melvile, 1982; Berberian & Yeats, 1999, 2001). Circles are instrumental earthquakes by Engdahl et al. (2006). Dashed ellipses show affected regions by the 1593, 1721, 1780, and 1786 historical earthquakes. Fault names are: ASF: Astaneh, WAF: West Alborz, SQF: South Qoshadagh, GCF: Goshachay, NBF: North Bozkosh, SBF: South Bozkosh, NMF: North Mishu, SMF: South Mishu, MGF: Maraghe, NKH: Nakhjavan, KHF: Khajeh, and NHF: Nehram. NTF is in thick solid line. (**b**) Circles: Seismicity recorded in IRSC network from 2006 until before the AVD. Colors represent hypocentral depths. Faults are the same as (a). Focal mechanisms with label are from the GCMT catalog until August 2020. Those labeled M6.1 ARD, M6.5 AVD1, M6.3 AVD2, and M5.9 TKC are from the 1997 Ardebil, 2012 AVD doublet and 2019 Mw5.9 Torkamanchay earthquakes. Triangles are the Tabriz permanent seismic sub-network stations belong to IRSC.

Figure 2. Seismicity along NTF and NMF. (**a**): black circles are the earthquakes from 2006 to before the 2012 AVD and white circles are the earthquakes that occurred after 2012 AVD until 2019 TKC. Ellipse is the estimated cumulative slip model for the creeping segment of NTF near SND from 1721 AD historical earthquake until AVD. The dashed circle is the thermal area (after Ghalamghash et al, 2019). (**b**) up: histogram showing seismicity selected in distance of 5 km

from NTF and NMF shown in (a). NMF stands for North Mishu Fault. down: Diagram of cumulative scalar seismic moments along NTF and NMF.

Figure 3. Transferred Coulomb stress field from the creeping segment of NTF on the (**a**) AVD ruptures and (**b**) the Western and Eastern segments of the creep segment of NTF, where high seismic activity was observed. The shown Coulomb stress fields are for the depth of 6 km. Circles along NTF are earthquakes from 2006 until AVD. The rest are early aftershocks of the AVD (IRSC). Dashed circle is the thermal area by Ghalamghash et al., (2019). Solid large circle shows the area of neo-Sahand young craters near Bostan Abad (BA). Dashed line marked A is the position of vertical cross sections shown in Figures 5 and 6.

Figure 4. (**a**): Transferred Coulomb stress fields from AVD ruptures on NTF (up: EV#1, down: EV#2). (**b**): Transferred Normal stress fields from AVD ruptures on NTF (up: EV#1, down: EV#2). The shown stress fields are for the depth of 10 km.

Figure 5. Schematic plot illustrating the relation between SND magmatic activity, NTF creeping segment, and AVD ruptures (marked AV#1 & AV#2). Low and high velocity areas are from Bavali et al., (2016), Rezaeifar et al., (2016), and Ghalamghash et al, (2019) studies. Stars are the 11 August 2012 M6.5&M6.3 mainshocks centroids. Thick dashed line is the NTF. Horizontal dashed lines are crustal velocity layers from Momeni & Tatar, (2018).

Figure 6. Graphic illustration of triggering of the 2012 AVD by the transfer of Coulomb stress field produced by the central NTF creeping segment. Stars are the mainshocks hypocenters.

Rupture models are from Momeni et al., (2019). Horizontal dashed lines are crustal velocity layers from Momeni & Tatar, (2018).

Figures:

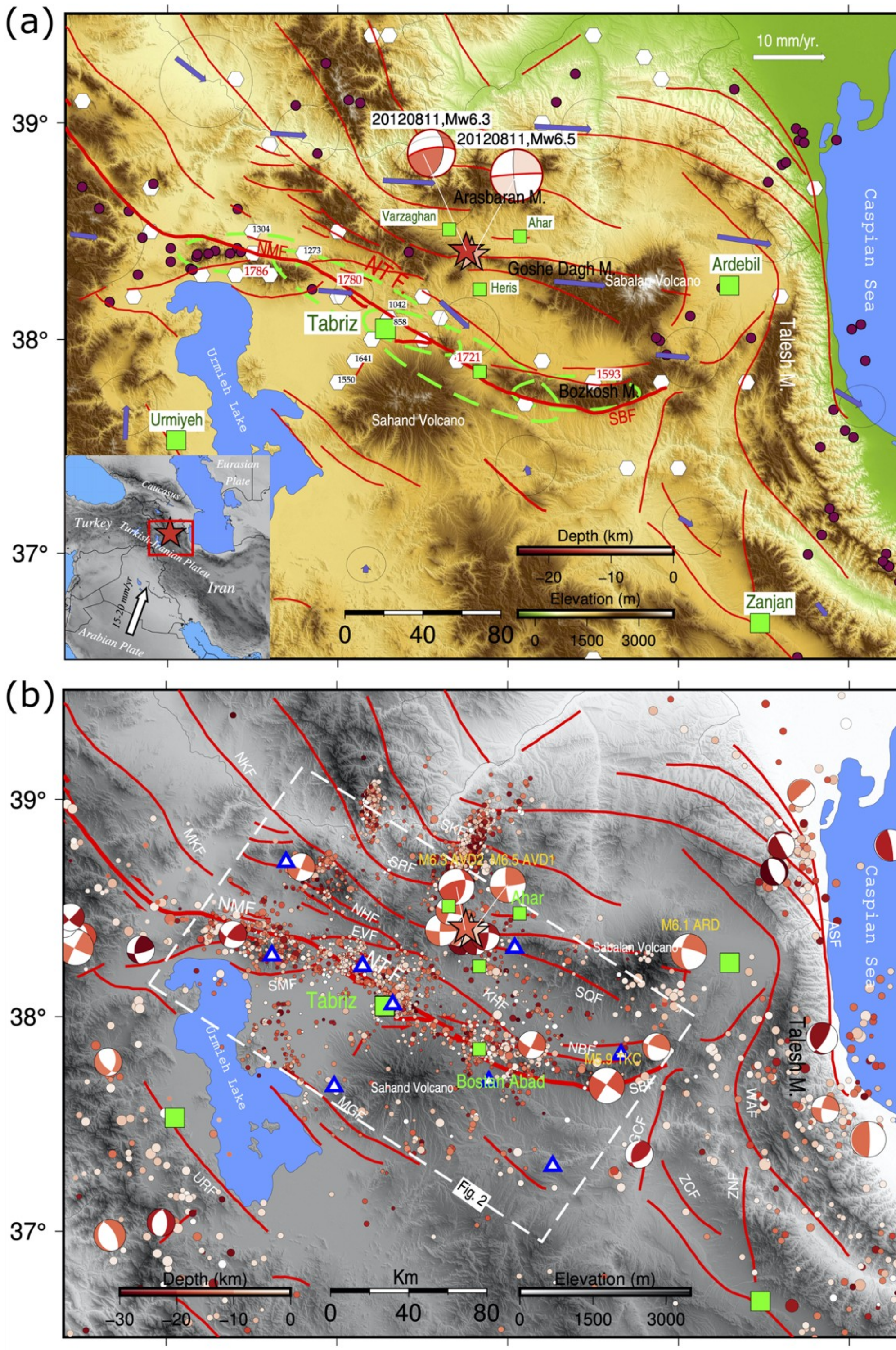

Figure 1. (**a)** Seismotectonics of the study region. **(b)** Seismicity recorded in IRSC network from 2006 until before the AVD.

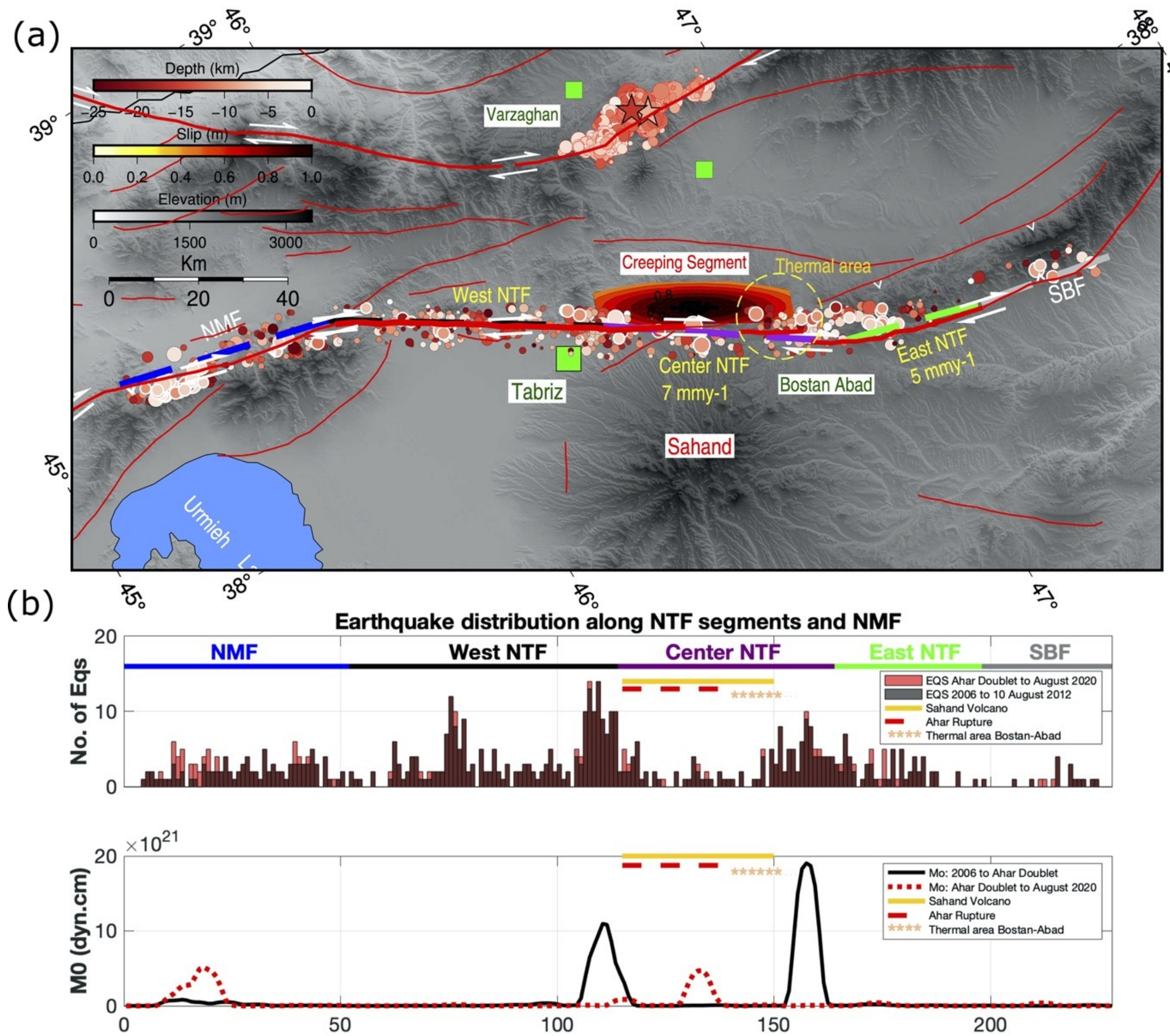

Figure 2. **(a)** Seismicity along NTF and NMF. **(b)** Histograms of earthquake distribution along NTF and NMF.

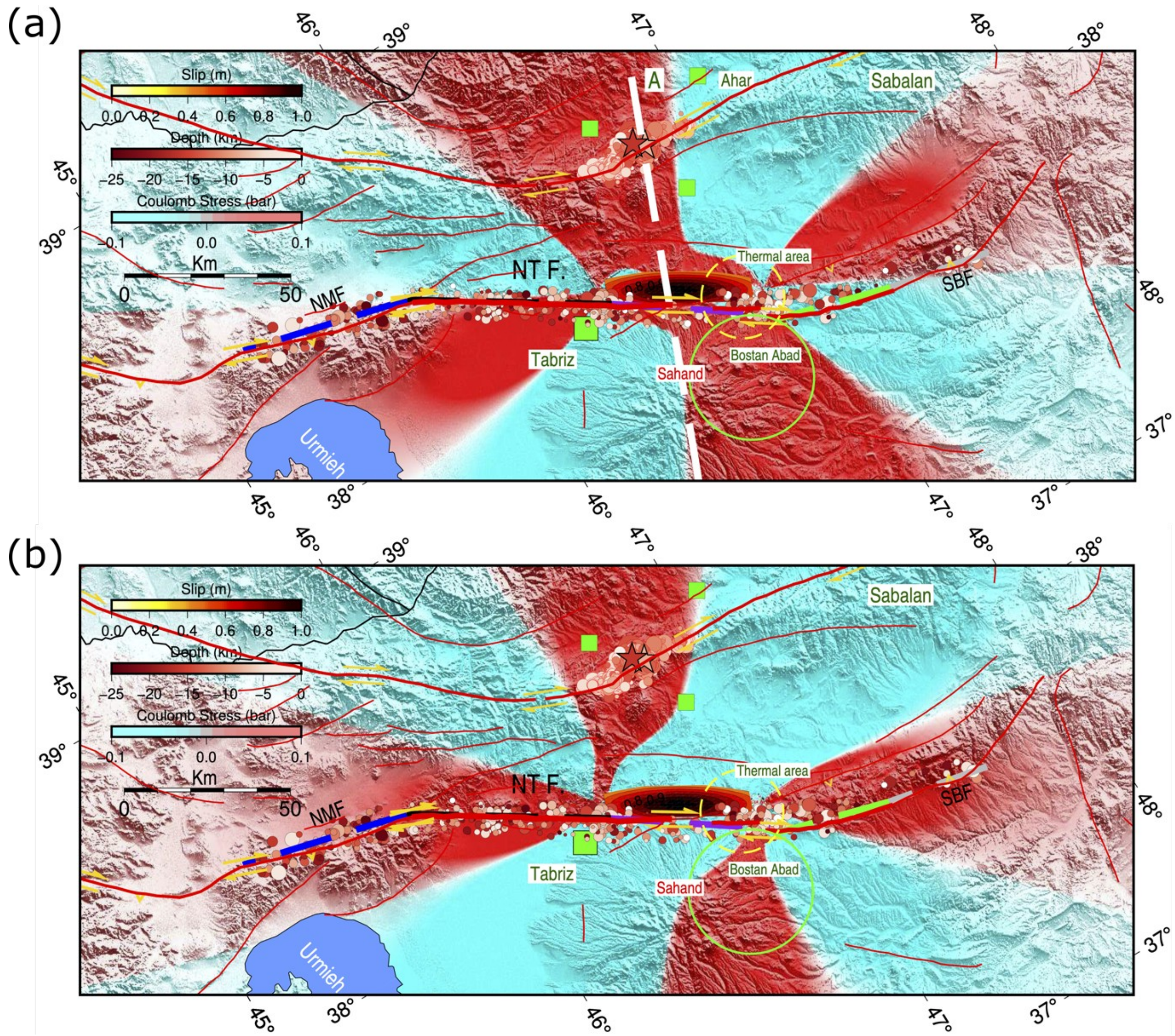

Figure 3. Transferred Coulomb stress field from the creeping segment of NTF. **(a)** on the AVD ruptures and **(b)** on the Western and Eastern segments of the creeping segment.

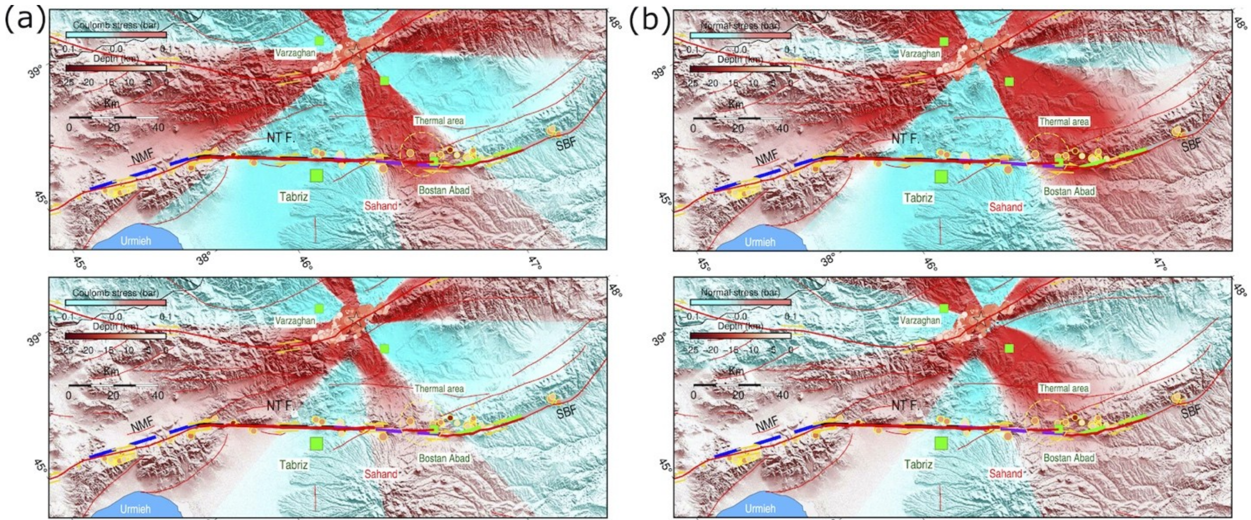

Figure 4. Transferred **(a)** Coulomb and **(b)** Normal stress fields from AVD ruptures on NTF.

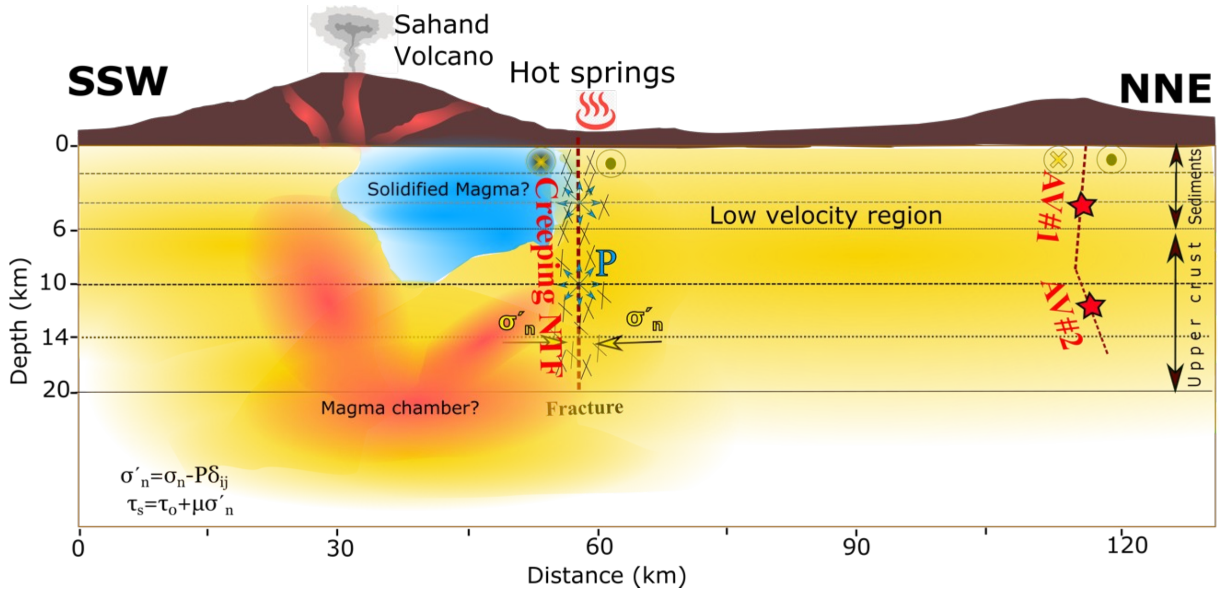

Figure 5. Schematic plot illustrating the relation between SND magmatic activity, NTF creeping segment, and AVD ruptures.

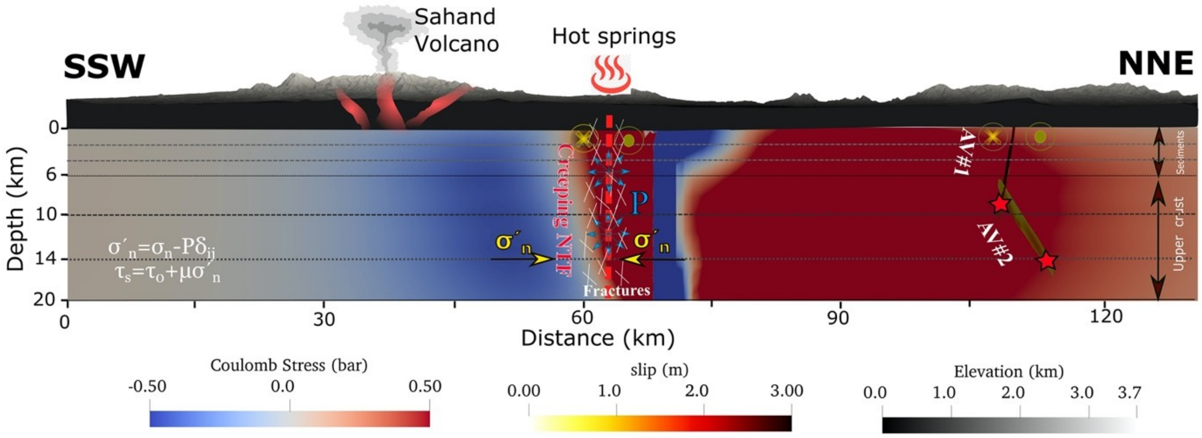

Figure 6. Graphic illustration of triggering of the 2012 AVD by the transfer of Coulomb stress field produced by the central NTF creeping segment.

Electronic Supplement

Tables:

Table S1. Velocity model of the NW Iran by Momeni & Tatar, (2018).

Depth of layer top	Vp	Vs
-3	4.58	2.44
2	5.65	3.11
4	5.92	3.34
6	6.20	3.53
10	6.35	3.63
14	6.52	3.71
46	8.10	4.63

Table S2. Earthquakes with Ml>=2.5 along the North Tabriz fault segments and NMF and SBF from 2006 until before the August 2012 Ahar-Varzaghan earthquake doublet (Mw6.5&6.3) (IRSC).

	Longitude	Latitude	Year	Month	Day	Magnitude	Depth	Hour	Minute
Central NTF	46.56	37.95	2007	10	4	2.7	12.80	3	2
	46.43	38.09	2007	12	1	4.5	7.4	18	45
	46.64	37.94	2008	3	24	3.1	11.8	9	44
	46.42	38.10	2008	4	7	3.2	11.4	2	48
	46.42	38.09	2008	5	10	3.3	15.1	16	15
	46.57	37.96	2009	6	13	2.7	15.5	23	21
	46.82	37.87	2009	10	12	2.7	9.8	20	55
	46.84	37.86	2010	2	2	3.6	5.0	10	5
	46.84	37.83	2010	2	2	3.4	2.1	10	15
	46.84	37.86	2010	2	2	4.6	5.0	10	16
	46.83	37.84	2010	2	2	3.8	5.0	11	26
Eastern NTF	47.21	37.72	2006	2	2	2.9	8.4	19	49
	46.99	37.81	2007	5	26	2.5	8.4	22	1
	47	37.73	2007	6	21	2.7	3.5	16	27
	46.97	37.82	2008	1	28	2.8	5.4	13	38
	47.13	37.73	2008	4	19	3.1	18	13	36
	46.88	37.84	2010	2	2	3.0	11.6	13	23
	47.04	37.77	2011	10	18	2.9	1.7	21	4
Western NTF	46.22	38.20	2006	1	8	3.1	4.0	17	19
	46.34	38.07	2008	1	22	2.5	10	8	55
	46.34	38.14	2008	6	1	2.6	13.50	2	17
	46.18	38.16	2008	6	26	2.6	16.20	16	34
	46.20	38.15	2008	6	26	2.6	14.70	16	39
	46.18	38.16	2008	6	26	3.1	16.70	17	6
	46.18	38.16	2008	6	26	2.7	15.80	17	8
	46.35	38.13	2008	7	28	2.9	17.20	7	13
	46.10	38.23	2009	2	13	2.6	5.1	4	0
	46.39	38.11	2009	8	5	2.6	10.40	22	15
	45.93	38.29	2010	1	4	2.6	10	7	38
	46.34	38.12	2011	1	29	3	14.80	7	29
	46.36	38.10	2012	5	4	2.6	7.8	21	48
NMF	45.47	38.41	2006	8	12	3.6	13.60	7	2
	45.35	38.49	2007	7	8	2.6	15.80	22	49
	45.38	38.40	2008	4	22	3.7	9	19	53
	45.74	38.34	2008	9	6	2.6	3	11	8
	45.41	38.47	2009	4	24	3.6	3.8	18	28
	45.45	38.39	2011	8	19	2.6	19.8	4	31
	45.69	38.36	2012	2	5	2.9	23.6	22	15
	45.57	38.43	2012	4	29	3.2	8	0	16
	45.55	38.42	2012	4	29	3	11.20	0	22
SBF	47.55	37.64	2008	6	12	2.5	10	3	19
	47.29	37.75	2010	7	14	2.9	18	16	46
	47.54	37.68	2010	10	23	2.7	4.10	17	59
	47.55	37.66	2011	6	6	3.1	0.70	12	23
	47.55	37.64	2008	6	12	2.5	10	3	19

Table S3. Earthquakes with Ml>=2.5 along the North Tabriz fault segments and NMF and SBF from the August 2012 Ahar-Varzaghan earthquake doublet until the November 2019 Mw5.9 Torkamanchay earthquake (IRSC).

	Longitude	Latitude	Year	Month	Day	Magnitude	Depth	Hour	Minute
Central NTF	46.47	38.06	2012	12	13	2.7	18	0	29
	46.75	37.93	2012	12	16	3.2	10	10	41
	46.42	38.09	2014	3	9	3.6	7.4	6	34
	46.59	37.93	2015	1	19	3.8	9.5	11	53
	46.84	37.87	2015	12	2	2.8	8	0	31
	46.52	38.00	2016	1	27	3.0	14.7	20	31
	46.43	38.04	2016	6	27	2.5	19.6	18	38
	46.42	38.03	2017	1	5	2.6	5.7	4	33
	46.43	38.06	2018	12	12	3.5	6	5	56
	46.44	38.07	2018	12	21	3.6	5	9	39
	46.60	37.98	2019	8	16	4.2	8.9	10	55
Eastern NTF	47.03	37.80	2013	2	8	2.6	10	19	25
	46.95	37.82	2013	2	12	2.5	5.1	8	11
	47.05	37.76	2014	2	11	2.7	5.4	10	18
	47.04	37.77	2014	8	19	2.5	10	5	43
	47.02	37.78	2014	9	8	2.8	10	16	53
	47.04	37.80	2018	6	1	2.5	10	0	8
	46.99	37.79	2018	11	24	3.3	8.6	17	22
	47.01	37.78	2018	11	25	2.5	10	9	46
	47.00	37.78	2018	11	26	3.3	6	20	9
	46.99	37.79	2018	11	27	2.7	6	11	33
Western NTF	45.89	38.29	2013	10	12	2.9	6	5	48
	45.90	38.35	2015	2	5	2.5	6.9	7	40
	46.38	38.13	2015	4	4	2.8	10	21	24
	45.97	38.30	2016	10	28	2.7	19.3	9	18
	46.31	38.07	2016	11	14	3.6	7.6	3	35
	45.98	38.28	2016	12	29	2.6	10	8	36
	46.34	38.12	2017	3	31	2.7	10	20	4
	46.32	38.07	2017	6	23	2.6	8	4	35
	46.04	38.23	2018	1	22	3.2	8.4	15	59
	46.04	38.23	2018	1	22	2.9	9.4	16	14
	46.34	38.14	2018	5	6	2.7	9.4	8	33
	46.36	38.11	2018	6	22	2.9	10	17	5
	46.34	38.13	2019	5	8	2.9	8.9	22	57
NMF	45.36	38.43	2013	4	18	4.9	6.1	10	39
	45.34	38.41	2013	4	18	3	10.2	10	53
	45.35	38.42	2013	4	18	2.9	12	11	32
	45.38	38.41	2013	4	18	3.9	6.4	11	40
	45.33	38.42	2013	4	18	2.6	30.3	13	30
	45.39	38.40	2013	4	29	2.6	12.6	14	36
	45.41	38.40	2013	6	28	4.2	5.30	5	13

	45.46	38.45	2014	3	12	2.6	10.8	10	28
	45.60	38.43	2014	5	13	2.5	9.8	3	59
	45.30	38.44	2015	4	10	2.5	10	19	17
	45.75	38.34	2015	12	31	3	11.8	22	31
	45.65	38.37	2016	2	15	2.5	7.3	4	56
	45.67	38.39	2016	9	26	2.5	8	20	35
	45.71	38.35	2016	9	27	3.7	5	18	18
	45.67	38.38	2016	10	7	2.6	4	7	13
	45.40	38.40	2016	12	26	2.9	18.3	1	55
	45.34	38.41	2017	12	4	2.5	7	7	0
	45.37	38.43	2018	1	13	3.2	6	0	50
	45.69	38.38	2018	3	4	2.6	6	8	16
	45.33	38.41	2018	3	30	2.7	4	10	10
	45.40	38.41	2018	4	30	3.4	11	5	49
	45.66	38.38	2018	6	19	2.6	9	2	56
	45.66	38.38	2018	9	4	2.6	6.4	1	50
	45.42	38.41	2018	11	21	3.3	5	0	42
	45.45	38.42	2018	12	26	3.5	5	7	41
	45.33	38.42	2019	4	11	2.7	10	9	14
	45.33	38.42	2019	4	12	3.4	6	0	16
	45.35	38.43	2019	4	12	3.8	6	4	12
	45.33	38.43	2019	4	12	2.7	6	6	14
	45.39	38.40	2019	6	8	2.8	6	0	54
	45.44	38.39	2019	6	8	2.5	6	1	0
	45.44	38.43	2019	6	9	2.8	4.9	4	14
SBF	47.47	37.67	2013	1	15	2.7	13.1	5	31
	47.42	37.71	2015	12	28	3.5	9	10	3
	47.44	37.71	2019	4	15	2.7	6.8	6	22